March 2016

Modeling Interactions Between Human Factors and Traffic Flow Characteristics

Chaoqun Jia
University of Massachusetts Amherst

MODELING INTERACTIONS BETWEEN HUMAN FACTORS AND TRAFFIC FLOW CHARACTERISTICS

A Dissertation Presented

by

CHAOQUN JIA

Submitted to the Graduate School of the
University of Massachusetts Amherst in partial fulfillment
of the requirements for the degree of

DOCTOR OF PHILOSOPHY

February 2016

Civil and Environmental Engineering

MODELING INTERACTIONS BETWEEN HUMAN FACTORS AND TRAFFIC FLOW CHARACTERISTICS

A Dissertation Presented

by

CHAOQUN JIA

Approved as to style and content by:

Daiheng Ni, Chair

John Collura, Member

Weibo Gong, Member

Richard Palmer, Department Chair
Civil and Environmental Engineering

DEDICATION

Dedicated to my beloved parents, my adviser and my friends.

ACKNOWLEDGMENTS

Thank Dr. Daiheng Ni for his supervision and support during my study in UMass Amherst. Thank Dr. John Collura, Dr. Weibo Gong, my thesis members, for their contributions to my dissertation. Thank my parents and friends for their always being there.

ABSTRACT

MODELING INTERACTIONS BETWEEN HUMAN FACTORS AND TRAFFIC FLOW CHARACTERISTICS

FEBRUARY 2016

CHAOQUN JIA

B.Sc., XIAN JIAOTONG UNIVERSITY

M.Sc., UNIVERSITY OF MASSACHUSETTS AMHERST

Ph.D., UNIVERSITY OF MASSACHUSETTS AMHERST

Directed by: Professor Daiheng Ni

To serve research needs for traffic flow model development and highway safety enhancement, we model interactions between human factors and traffic flow characteristics, this topic includes methods on collecting data, modeling impacts of parameters on flow, and calibrating parameters on observed data. An example of successful traffic data collection is NGSIM data, which contains location, speed, and acceleration information of vehicles. An algorithm was designed to match and extract vehicles' trajectory records, and utilize the extracted information for pattern recognition of lane changing maneuvers. This algorithm reads records from an NGSIM data set, pick out vehicles executing lane changing maneuvers, and note the corresponding time stamps. Also through matching these records by vehicle ID and time stamp, we obtain a map of vehicles when a lane changing is happening, thus calculating gaps and relative speeds becomes possible. An example of utilizing these information is

pattern recognition on lane changing maneuvers. We analyze lane changing maneuvers with speed data and gap data. The approach with speed data shows convincing results, as most lane changing vehicles have a descending and then ascending pattern on their speed profiles before executing the maneuver. On the other hand we can use collected data for calibrating parameters in traffic flow models. A heuristic methodology is implemented to provide results with high accuracy, high efficiency and high robustness. Techniques include data aggregation and bisection analysis are applied in this approach to ensure achieving these goals and further requirements. Two traffic flow simulation models, Longitudinal Control Model (LCM) and Newell's Model are calibrated by applying this approach using traffic data collected at Georgia 400 highway in July, 2003, with satisfying accuracy and robustness produced in a running time of less than 2 seconds. Meanwhile we can enhance human factors by applying new technologies, and connected vehicle is a good example which is rapidly developing. Future vehicles will be able to communicate with each other which greatly improves drivers' situational awareness. Consequently, drivers may be able to respond earlier to safety hazards before they manifest themselves in forms of imminent danger. Therefore, the overall effect of this technology can be attributed to drivers' enhanced perception-reaction (P-R) capability which, in turn, translates to improved flow and capacity. However, it is critical to quantify such benefits before large-scale investment is made. In our research, a statistical transformation model is formulated to predict the probability distribution function of flow. By entering distributions of P-R time and enhanced P-R time, this model helps compare before and after distributions of traffic flow, based on which benefits of connected vehicles on traffic flow can be analyzed.

TABLE OF CONTENTS

LIST OF TABLES

Table **Page**

LIST OF FIGURES

Figure **Page**

CHAPTER 1

INTRODUCTION

1.1 Motivation: safety problems caused by human factors

Every year around 1.2 million people are killed in road accidents all over the world, and another 50 million get injured for Statistics & Analysis (2010). Among these tragedies, many are caused by aggressive driving in severe conditions require extra carefulness, such like bad weather, road sections near work zone or crash site, etc. Usually people have their consistent driving styles, which can be described by a traffic flow model, and under a special situation it's not guaranteed a driver adjusts his/her style properly in corresponding to the change of situations happened on road. For example, a proportion of drives failed to drive more carefully near work zones, and this is a remarkable source of accidents Pigman & Agent (1990). And during conditions of light precipitation, friction between tyres and pavement deteriorates significantly, but drivers not experienced enough might be not sure how careful they should be. Under such a circumstance an un-experienced driver has a high probability to drive in an overly aggressive style. As a result, an investigation conducted by FHWA FHWA (2011) suggests that an average annual rate for weather related crashes from 1995 to 2008 is approximately 1.5 million, this number counts for 24% of all vehicle crashes annually. And during the same period more than 7 thousands people were killed on road every year, which counts for 17% of all crash fatalities. These statistics can be found in the following table 1.1.

Meanwhile, as electrical technologies developing, researchers now have sensing and computing capacities more powerful than ever before. With these powerful develop-

Table 1.1 Weather-Related Crash Statistics (Annual Averages 1995-2008) FHWA (2011)

Road Weather Conditions	**Weather-related Crash Statistics**		
	Annual Rates (Approximately)	**Percentages**	
Wet Pavement	1,128,000 crashes	18% of vehicle crashes	75% of weather-related crashes
	507,900 persons injured	17% of crash injuries	81% of weather-related crash injuries
	5,500 persons killed	13% of crash fatalities	77% of weather-related crash fatalities
Rain	707,000 crashes	11% of vehicle crashes	47% of weather-related crashes
	330,200 persons injured	11% of crash injuries	52% of weather-related crash injuries
	3,300 persons killed	8% of crash fatalities	46% of weather-related crash fatalities
Snow/Sleet	225,000 crashes	4% of vehicle crashes	15% of weather-related crashes
	70,900 persons injured	2% of crash injuries	11% of weather-related crash injuries
	870 persons killed	2% of crash fatalities	12% of weather-related crash fatalities
Icy Pavement	190,100 crashes	3% of vehicle crashes	13% of weather-related crashes
	62,700 persons injured	2% of crash injuries	10% of weather-related crash injuries
	680 persons killed	2% of crash fatalities	10% of weather-related crash fatalities
Snow/Slushy Pavement	168,300 crashes	3% of vehicle crashes	11% of weather-related crashes
	47,700 persons injured	2% of crash injuries	8% of weather-related crash injuries
	620 persons killed	1% of crash fatalities	9% of weather-related crash fatalities
Fog	38,000 crashes	1% of vehicle crashes	3% of weather-related crashes
	15,600 persons injured	1% of crash injuries	2% of weather-related crash injuries
	600 persons killed	1% of crash fatalities	8% of weather-related crash fatalities
Weather-Related	**1,511,200 crashes**	**24% of vehicle crashes**	
	629,300 persons injured	**21% of crash injuries**	
	7,130 persons killed	**17% of crash fatalities**	

ments come new methods on collecting and modeling traffic flow data, and calibrating models. Thus extracting information from observed raw data supports further study of traffic behaviors, and from these empirical data we can calibrate parameters of existing models. Our work focus on quantifying the interactions between human factor parameters and highway traffic flow.

1.2 NGSIM Project

As an example of traffic data collection, the Next Generation SIMulation (NGSIM) project was initiated by United State Department of Transportation (USDOT) Federal HighWay Administration (FHWA) in 2002, aiming on collecting detailed vehicle trajectory data for various research purposes including FHWA (2006b): producing data sets that can be used for research and development in simulation community, and making outputs of this project publicly available to researchers in simulation and other communities. Alongside FHWA, this project is also supported by three stakeholder groups FHWA (2006a), including a traffic modelers group, a software developers group, and model users group. Members of these groups are also constitute traffic flow microsimulation communities, including academic research community and commercial microsimulation developing companies. After assessing existing microsimulation models for traffic flow, the NGSIM team formulated high-level plans which include data plan, algorithm plan, and validation plan. These plans detailed methodologies for tasks include field data collection, essential microsimulation model development, and model validation by applying simulation software packages.

The first location surveyed by NGSIM was a section of Interstate 80 in Emeryville, California, near Pacific Park Plaza Thiemann et al. (2008) FHWA (2006a). To implement this data collecting project, cameras were installed on top of Pacific Park Plaza, as shown in figure 1.1, in which a digital camera was mounted towards north bound of Interstate 80. Videos recorded by cameras were processed by graphical pro-

cessing software afterwards and vehicle trajectory data were extracted into plain text files, including vehicles' positions, speeds, accelerations, and gaps between them, etc. First experiment was conducted in December 2003 Thiemann et al. (2008), with 4,733 vehicles recorded in a 30-minute video. Another data set at the same location was collected in April 2005 Thiemann et al. (2008), with 5,648 vehicles recorded in three 15-minute videos. Following these two data set collections, traffic data were also collected on US-101 in Studio City, California, on Peachtree Street in Atlanta, Georgia, and on Lankershim Blvd, Los Angles, California. All these data set collections were conducted by Cambridge Systematics, Inc. in Oakland, California.

Figure 1.1 A camera installed on top of Pacific Park Plaza recording vehicle trajectory data FHWA (2006a)

Another category of products from NGSIM project are simulation algorithms, including car-following and lane changing models FHWA (2006a). These models were developed based on previously mentioned data sets, and can be used to improve current simulation models. Also corresponding detailed documentations are included to explain these algorithms and models. All these outputs of NGSIM project are provided to researchers freely and publicly.

1.3 Modeling impact of human factor improvements

As connected vehicle technology rapidly developing, future vehicles will be able to communicate with each other which greatly improves drivers' situational awareness. Consequently, drivers assisted by the technology may be able to respond earlier to safety hazards before they manifest themselves in forms of imminent danger, which results decreased mean perception-reaction (P-R) time. While the help to young and skilled drivers may not sound significant, drivers who are somehow impaired and necessitate longer P-R times can benefit more from the technology. As such, their tend to perform better in responding, and hence lower their mean and standard deviation of P-R time. Therefore, the overall effect of this technology can be attributed to drivers' enhanced perception-reaction (P-R) capability which, in turn, translates to improved flow and capacity. For example, drivers may take advantage of the enhancement as follows:

- Enjoy more safety buffer by keeping the same headways in front of them as before.
- Maximize flow rate by following leaders closer while keeping the same safety buffer as before.

Obviously in the real world, drivers' choices might be a mixture of the two involving a trade-off between safety and flow. In order to quantify the flow benefit, one needs to understand the role of P-R time in drivers' control behavior, especially in car following. Many models have been proposed such as Forbes Forbes & Simpson (1968), Gipps Gipps (1981), and Ni Ni (2011a). Building on driver behavior models, we derived a statistical transformation that relates a distribution of P-R time to a distribution of flow. Consequently, an enhancement in P-R time can be quantitatively translated into an improvement of flow and capacity. Recognizing that the underlying driver behavior model and distribution of P-R time may vary for different analysts

and calibrating data sets, the objective of this paper is to propose a methodology that does not depend on the models and distributions discussed herein. As such, analysts may customize the methodology according to their specific nature and use it to quantify flow benefits before large-scale investment on connected vehicle technology is made.

1.4 Thesis Contributions

Our contributions to the traffic flow modeling community are summarized as following aspects:

- We make it easier and more efficient to extract traffic information from NGSIM data. An information extraction algorithm is designed to match and output vehicles' trajectory records, and the output of this algorithm are utilized for further research on lane changing maneuvers.

- From empirical traffic data sets, based on distribution numerical search principles, an efficient method is designed and developed to calibrate traffic flow model parameters. This calibration is efficient enough for reporting human factor parameter values in real time, and thus provide an option on highway safety surveillance.

- From known or assumed human factor parameter values, based on distribution transformation principle, a model on predicting impact of human factor improvement on traffic flow characteristics is developed. As an example of this model's application, considering P-R time enhancement introduced by connected vehicle technology, the potential improvement on highway traffic flow was quantified.

1.5 Thesis Organization

This thesis is organized as follows.

We first introduce the motivation and backgrounds of our research, including safety concerns caused by human factors, NGSIM data collection project, and how human factor enhancement can help improve traffic flow characteristics.

In Chapter 2, a brief review on related topics is demonstrated. These topics include: previous work on traffic data collection methods and resulting data sets, traffic flow models and calibration methods, and models on human factors like P-R time.

In Chapter 3, we first illustrate how P-R time can have an impact on traffic flow characteristics, and then three parts of our work are presented, including: NGSIM data decomposition and lane changing information extraction, structure of the calibration algorithm for determining human factor parameters from empirical data sets, and derivation for modeling impact of human factor parameters on traffic flow characteristics.

In Chapter 4, we show implements of methodologies mentioned in Chapter 3, and corresponding results. Further analysis on results are discussed.

In Chapter 5, we give a summary of the work in this thesis.

CHAPTER 2

LITERATURE REVIEW

2.1 Traffic data collection methods

Collecting traffic flow data, especially vehicle trajectory data, has been an important topic in traffic flow theory research community and simulation development community. As early as in 1950's, Chandler et al. Chandler et al. (1958a) and Herman et al. Herman & Potts (1959) in General Motors connected vehicle pairs with wires to measure spacing, relative speed and acceleration. They conducted experiments on different road conditions and successfully collected data for car-following researches.

In recent years, new technologies are contributing in traffic data collections. Global Positioning System (GPS) provides precise position information of vehicles. Gurusinghe et al. Gurusinghe et al. (2002) and Punzo et al. Punzo & Simonelli (2005) tested methods of using GPS for position obtaining on test tracks and real roads, and useful data were collected. However, in a near future, this method cannot be implemented for collecting big size empirical data sets, because not all vehicles are equipped with GPS-enabled devices.

As an intuitive way, using cameras for collecting traffic data has a long history since beginning of traffic flow theory research. In late 1950s, Kometani et al. Kometani & Sasaki (1959) experimented aerial camera shooting as the method to obtain traffic flow data, and proved it to be effective. Also this data collecting method was adopted and refined by Treiterer et al. Treiterer & Mayers (1974) and Xing Xing (1995). In 2004, Hoogendoorn et al. Hoogendoorn et al. (2004) tested a camera mounted on a helicopter and obtained detailed information on vehicle including longitudinal and

lateral positions, length and widths of vehicles. These information were collected with a resolution of 22 cm, and 94 % of vehicles in experiment sites were recognized and tracked automatically. Also cameras can be mounted on buildings to avoid problems for stabilizing an aerial vehicle. This strategy was adopted by Coifman et al. Coifman et al. (1998) while testing their vehicle recognizing software, on State Highway 99 in Sacramento, California, in 1998. Thus as technologies, especially computational graphics techniques, have developed to a stage that it is possible to use computers to recognize vehicle trajectories in videos. This fact makes projects like NGSIM possible.

After NGSIM project was conducted and its data sets were available to public, researchers in simulation community made efforts on utilizing these data. Ni Ni (2006) commented that NGSIM data sets have more details which help effective simulations. A. Duret et al. Duret et al. (2008) examined the data set of I80 collected during evening peak hour, and analyzes car-following behaviour patterns under congested conditions. Other similar models for drivers' behaviours in congestions designed by Yeo et al. Yeo et al. (2008) and Laval et al. Laval & Leclercq (2010), were developed using vehicle trajectory data from NGSIM.

By analysing NGSIM trajectory data with time series techniques, C. Thiemann et al. Thiemann et al. (2008) found NGSIM data has much less noise compared to traditional stationary detectors. F. Cunto et al. Cunto & Saccomanno (2008) Used NGSIM trajectory data to calibrate and validate a heuristic algorithm for evaluating safety measures at signalized intersections, and the algorithm was proved to be objective and efficient.

2.2 Traffic Flow Models and Calibration Methods

2.2.1 Traffic Flow Modeling and Calibrating

Pursuing of a precise mathematical model to describe traffic flow behaviours has lasted for more than half a century, and there are models successfully developed and

applied. Greenshields' model Greenshields et al. (1935) applies a simple linear relationship to traffic density and average speed, which is not precise enough but worked as the very beginning of research on modelling traffic flow characters. Newell's model Newell (1961) Newell (1993) has a much more precise description of traffic behaviours. General Motors Model Chandler et al. (1958b) Gazis et al. (1959) were developed as a car-following model but can be used as a tool for research on macroscopic traffic flow theories. Similarly Gipps' Model Gipps (1981) is a successful development on drawing how traffic's flow, density and average speed depend on each other. In Kosonen's Ph.D. dissertation Kosonen (1999), a rule-based model was applied in simulating traffic behaviours in urban environment, and this was based on previous research on utilizing fuzzy decision rules to simulate traffic flow Kikuchi & Chakroborty (1992). As the latest achievement on modelling traffic flows, Daiheng Ni Ni (2006) Ni (2011b) Ni (2011a) utilized field theory to simulate behaviours of vehicles on road, and got the Longitudinal Control Model (LCM), which we will introduce in details.

On the calibration part, there are also previous works trying to locate sufficient and precise methods for finding values of parameters in traffic flow models. This field of research was initiated by Chandler and Herman et. al Chandler et al. (1958b) Gazis et al. (1959), Herman & Potts (1959) at late 1950's and early 1960's. GM model was opted by Chandler's team and field data was studied for obtaining parameter values in the model. With development of computational technology, simulation tools are utilized in studying traffic phenomena and calibrating models, as revealed by Brackstone et. al. Brackstone & McDonald (1999). In the past decade there are several research projects improving calibration methods. Using field data obtained on IH-10 in Houston Texas, Schultz et. al. Schultz & Rilett (2004) evaluated the parameter values they calculated with microscopic traffic simulation tools. In 2008 Kesting et. al. Kesting & Treiber (2008) tested a method that minimizing the difference between field data and model prediction. They resulted with errors lower

than 30%. Also some ideas came from Computer Science helped getting a higher accuracy. Hoogendoorn et. al. Hoogendoorn et al. (2004) implemented genetic algorithm for calculating parameter values in traffic flow models in 2010.

2.2.2 Traffic Flow Models for Evaluating Drivers' Aggression

A suitable model for finding average aggression is Longitudinal Control Model (LCM) Ni (2006) Ni (2011b) Ni (2011a). In this macroscopic model we define relationship between traffic density and speed as:

$$k = \frac{1}{(\gamma v^2 + \tau v + l)[1 - \ln(1 - \frac{v}{v_f})]} \tag{2.1}$$

where k is traffic density, v is space-mean speed, γ denotes degree of aggression that characterizes the driving population, τ is average response time that characterizes the driving population, l is average effective vehicle length, and v_f is free flow speed. So if we get the value of γ against field data under a specific situation, current degree of aggression on road is found.

2.3 Perception-Reaction Time models

In the past decades, much work has been done on how to improve highway flow and safety. However, research on the impact of P-R time on highway safety has been focused on drunk driving Perrine et al. (1971) Wagenaar (1986), distraction Nasar et al. (2008) Royal (2003) Donmez et al. (2007), and aging Shinar et al. (2001) Williams & Carsten (1989) Stamatiadis & Deacon (1995) Lyman et al. (2002).

Research interests related to enhancing P-R time usually are on device and protocol development, rather than evaluating how the technology would improve flow. For example, Xu et al. Xu et al. (2003) designed a Vehicle to Vehicle (V2V) location-based

broadcast communication protocol in 2003 and tested it under different communication and highway conditions. In 2006 Biswas et al. Biswas et al. (2006) demonstrated a highway cooperation collision avoidance system, which is based on Dedicated Short Range Communication (DSRC) protocol and packet routing protocols used to support the application. Meanwhile, researchers have been working on enhancing the performance of V2V communication. Weinfield Weinfeld (2010) examined the DSRC protocol, described parameters that can reduce congestion in the wireless channel, developed methods to increase reliability of wireless communication, and obtained positive results in experiments.

In transportation community, flow and safety has always been the top priority. Vahidi et al. Vahidi & Eskandarian (2003) observed that improving car clusters leads to increased highway capacity. As such, automated vehicles can achieve large capacity since they are able to operate in compact platoons without compromising safety Michaud et al. (2006) Darbha & Rajagopal (1999), and field experiments seemed to support the observation H.-S. Tan (1998). However, there is a long way to go before automated vehicles become practical, the more feasible mode of operation in the near future is human drivers assisted by advanced technologies. Hence, the focus of this research is to evaluate the impact of P-R time enhancement such as that resulting from connected vehicle technology. Research efforts on similar topics have been reported but far from conclusive. For example, VanderWelf et al. VanderWerf et al. (2001) evaluated Cooperative Adaptive Cruise Control (CACC) and predicted large potential in capacity gain. In contrast, Autonomous Adaptive Cruise Control (AACC) could only have a much smaller impact on highway capacity. However Arem et al. van Arem et al. (2006) assessed some other scenarios of CACC and did not find much increase in capacity. In Arem's work, a traffic simulation model MIXIC was used to study the impact of CACC on a highway-merging scenario, and the result indicated only a slight increase in capacity. Based on a combination of traffic flow

modeling and statistical analysis, Ni et al. Ni et al. (2012) estimated how capacity would change as the percent of connected vehicles vary. Research by Nekoui Nekoui et al. (2011) concluded that V2V may achieve increased capacity by organizing denser vehicle platoons.

CHAPTER 3

METHODOLOGIES

3.1 The Role and effect of P-R time on Traffic Flow

In essence, human drivers constitute a delayed control system, that is, there is an inherent delay in drivers' response to the dynamic driving environment because of the time consumed during perception and reaction processes. As such, the delay is referred to as P-R time, and hence drivers need to maintain sufficient separation among them in order to account for the delay and ensure safety. Since different drivers perceive and react differently, their P-R times vary. In addition, even within the same driver, P-R time may change over time.

P-R time plays a role in virtually every aspect of driving including transient conditions such as acceleration/deceleration and stop-and-go processes and stable conditions such as coasting and car following. The effect of P-R time and further driving rules can be captured in mathematical models from a microscopic point of view. Many models have been proposed, among which we use the following models for illustration purpose.

As a good driving rule, Forbes Forbes & Simpson (1968) assumed that a vehicle must maintain a time separation of at least one P-R time from the leading vehicle, the following can be formulated under car-following condition:

$$s_{ij} \geq s_{ij}^{*} = \tau_i \dot{x}_i + l_j \tag{3.1}$$

where s_{ij} is the spacing between vehicle i and its leading vehicle j, s^*_{ij} is the desired value of s_{ij}, τ is P-R time, $\dot{x}$ is speed, and l is vehicle effective length. If vehicle i is not impeded by any other vehicles, it simply moves at its desired speed v_i and this constitutes the free flow condition:

$$\dot{x}_i = v_i \tag{3.2}$$

In this paper, our interest is flow and capacity, which is a macroscopic view point on traffic flow. Hence, the above microscopic model needs to be translated to the corresponding macroscopic version under steady state conditions:

$$q = \frac{1}{\tau}(1 - lk) \tag{3.3}$$

where q is, k is density, and flow is the product of traffic speed v and density: $q = vk$. Figure 3.1 illustrates the effect of P-R time captured in Forbes model. Scattered in the background are data points observed in the field showing the relationship between flow and density. Forbes model is used to approximate the empirical data. The top, middle, and bottom lines emitted from density at 200 veh/km are generated from Forbes model using P-R time τ = 1.0, 1.5, and 2.0 seconds respectively. The figure shows that the shorter the P-R time is, the higher the flow sustained. The line emitted from the origin are generated from the free flow condition $q = v_f k$ where v_f is free flow speed. The capacity is the maximum value of flow which is found as the intersection of the free-flow line and the car-following line. Obvious, shorter P-R time supports higher capacity. In this example, a ratio of P-R time of 1.0:1.5:2.0 seconds translates to a ratio of capacity of about 3070:2155:1666 veh/hr.

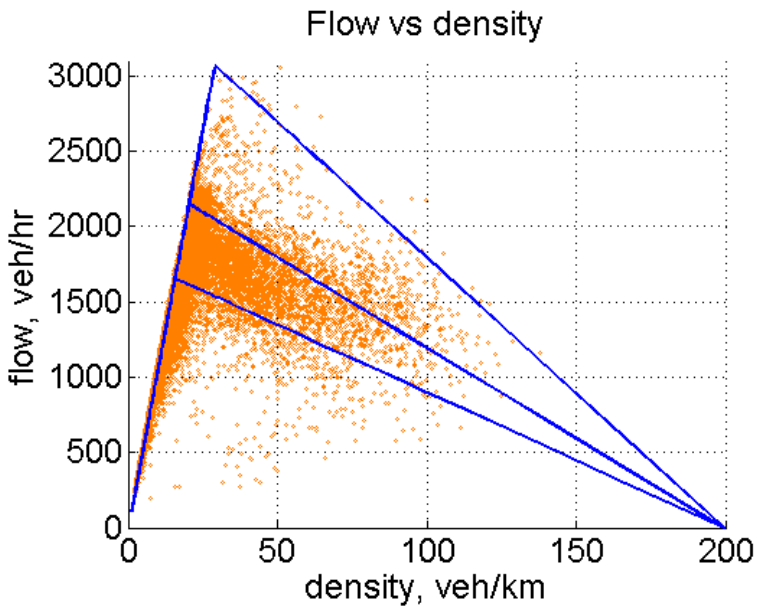

Figure 3.1 Effect of P-R time in Forbes model

As noted above, the role of P-R time takes effect through driving rules. Perhaps a safer driving rule can be the following which is assumed by Gipps Gipps (1981) in his model development: at any moment, a driver must leave enough room in front so that he could stop his vehicle safely after the perception and reaction processes should the leading driver applies emergency brake. A simplified formulation the above safe driving rule yields:

$$s_{ij} \geq s_{ij}^{*} = \frac{\dot{x}_i^2(t)}{2b_i} - \frac{\dot{x}_j^2(t)}{2B_j} + \dot{x}_i\tau_i + l_j \tag{3.4}$$

where B_j represents driver i's estimate of the emergency deceleration which is most likely to be applied by driver j, while b_i can be interpreted as the deceleration which driver i believes that he or she is capable of applying in an emergency. Note that the term $\frac{\dot{x}_i^2(t)}{2b_i} - \frac{\dot{x}_j^2(t)}{2B_j}$ represents degree of aggressiveness that driver i chooses. For example, when the two vehicles travel at the same speed, this term becomes $\gamma_i \dot{x}_i^2$ with:

$$\gamma_i = \frac{1}{2}(\frac{1}{b_i} - \frac{1}{B_j}) \tag{3.5}$$

Translating the above model to its corresponding macroscopic version under steady-state condition yields:

$$q = \frac{v}{(\gamma v^2 + \tau v + l)} \tag{3.6}$$

The above model is plotted in Figure 3.2 to illustrate the effect of P-R time against empirical data. The three curves from top to bottom are generated from the simplified Gipps model using P-R time τ = 1.0, 1.5, and 2.0 seconds respectively. Similar conclusion to that of Forbes model can be drawn about the effect of P-R time on flow, only the ratio of capacity becomes 2487:1849:1470 veh/hr in this example.

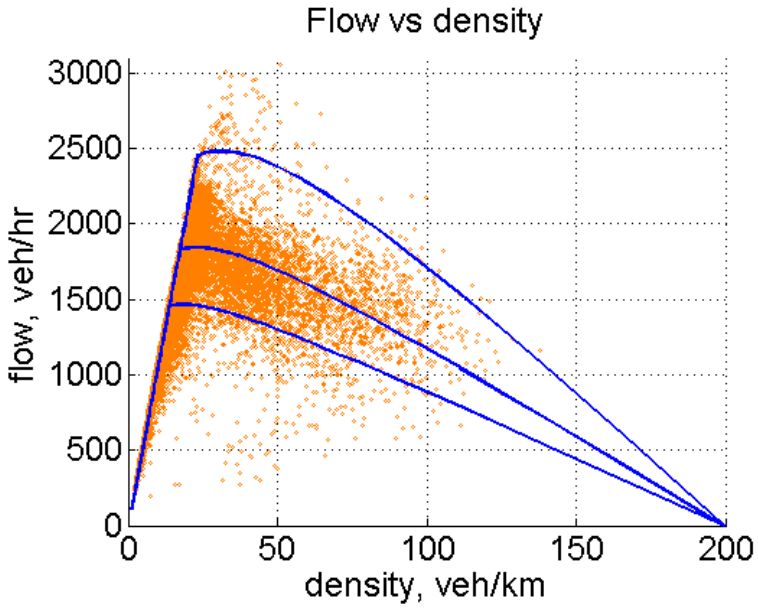

Figure 3.2 Effect of P-R time in simplified Gipps model

To be more realistic, the safe driving rule has been incorporated into the Longitudinal Control Model (LCM) Ni (2011a) with the understanding that b_i might

be greater than B_j in magnitude, which translates to the willingness (or aggressive characteristic) of driver i to take the risk of tailgating:

$$\ddot{x}_i(t+\tau_i) = A_i[1 - (\frac{\dot{x}_i(t)}{v_i}) - e^{1-\frac{s_{ij}(t)}{s^*_{ij}(t)}}] \tag{3.7}$$

where $\ddot{x}_i(t+\tau_i)$ is the operational control (acceleration or deceleration) of driver i executed after a perception-reaction time τ_i from the current moment t. A_i is the maximum acceleration desired by driver i when starting from standing still, other variables are as defined before.

Translating LCM to its corresponding macroscopic version under steady-state condition yields:

$$q = \frac{v}{(\gamma v^2 + \tau v + l)[1 - \ln(1 - \frac{v}{v_f})]} \tag{3.8}$$

Figure 3.3 illustrates the effect of P-R time in LCM model using the same set of τ values. Simular conclusion can be drawn from the figure only the ratio of capacity becomes 2788:1524:1157 veh/hr in this example.

Note that the three models discussed above are progressively complicated with a former model constituting a special case of the latter one. The matching of these models to empirical data confirms that P-R time does play a role in traffic flow with shorter P-R time supporting higher flow and capacity.

3.2 Structure of NGSIM data

Taking Interstate 80 in Emeryville as an example, this part of I80 has 4 to 6 lanes, and was included in NGSIM project. Figure 3.4 shows a segment of I80 near Pacific

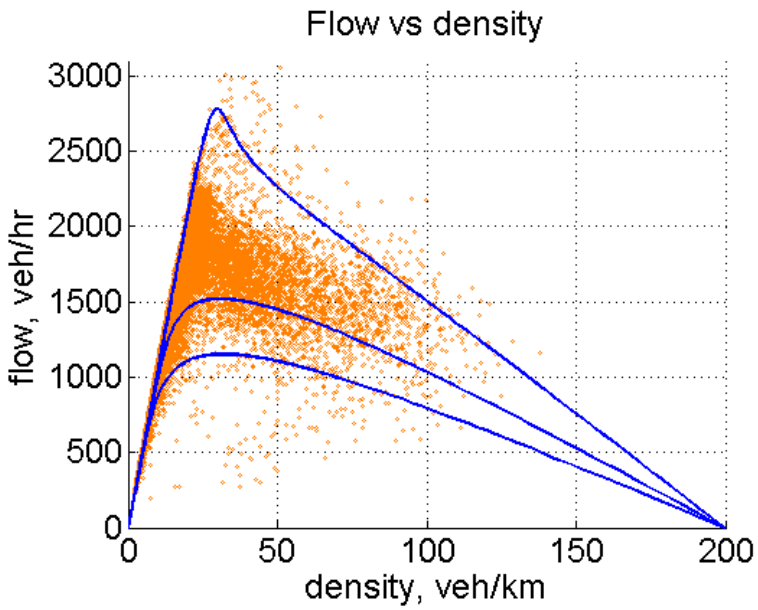

Figure 3.3 Effect of P-R time in LCM model

Park Plaza, California, 94608. In data set produced by NGSIM project, this segment can be modelled as shown in Figure 3.4.

The fundamental data collecting model is demonstrated in Figure 3.4. In a section of highway, lanes are tagged with numbers starting from the left side, and a Cartesian Coordinates System is constructed, with the most-left end of this section's entry side as the origin, and the section of highway is kept in the first quadrant. Coordinates of a vehicle are referred to its front middle point, both are positive. In this way the project obtains a vehicle's local coordination.

Based on this fundamental data collecting model, there are other useful information that can be derived from it. For every location, an aerial shot photo is taken every millisecond, so it's possible to calculate the numerical approximation of first and second order derivatives of every vehicle's distance from y axis. In other words, it's possible to get every vehicle's speed and acceleration from its local coordination.

Besides location, speed and acceleration, there are other information collected in this project. Vehicle ID is arbitrarily defined to identify data rows belong to a specific vehicle, vehicle width and length can be easily obtained. Vehicle class refers

to the category a vehicle is in: Motorcycle, Auto, or Truck. Global coordination is obtained by setting an origin for the entire region, so this is redundant information as it can be calculated from local coordinate and definition of highway sections. Other important information includes space headway, time headway, preceding vehicle ID and following vehicle ID, which are self-explanatory.

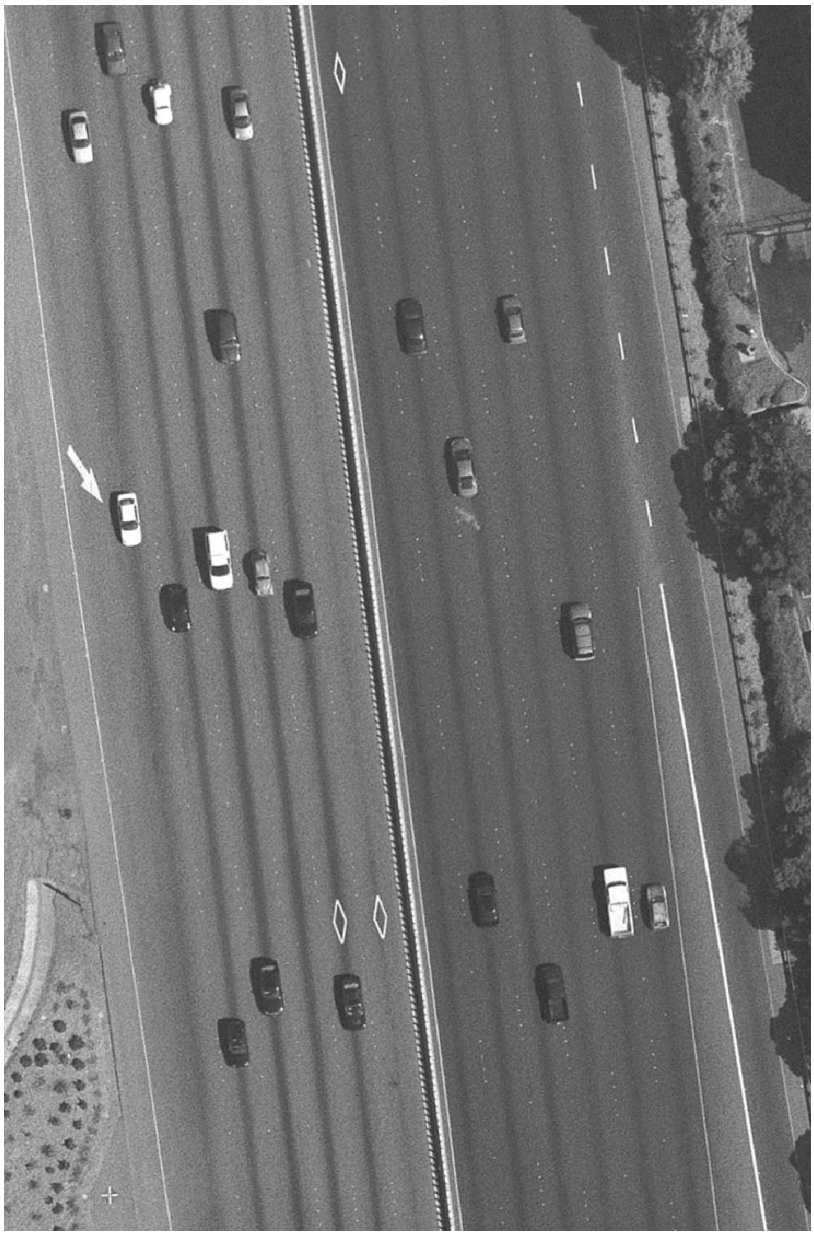

Figure 3.4 I80 near Pacific Park Plaza, Emeryville, CA

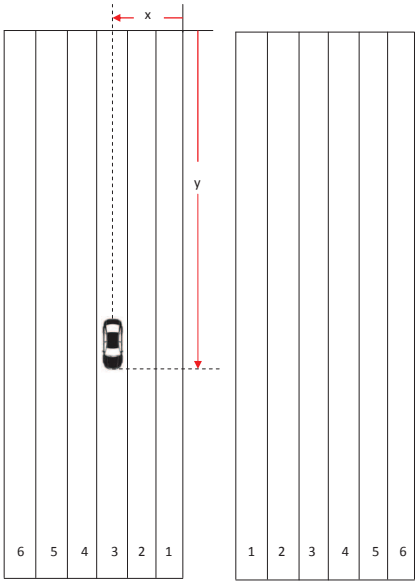

Figure 3.5 NGSIM model of I80 near Pacific Park Plaza, Emeryville, CA

In every NGSIM data set, all aerial shot frames for one shooting region are aggregated into one plain text file. Every row in this file is an entry of information for a vehicle in a frame. Information of the same vehicle for different frames are placed in neighbouring rows. A simple description of one data set's structure can be found in Table 3.2, where vid_i is the ID of ith vehicle, $t_{i,j}$ is the time when the jth row of information for ith vehicle is collected. $(x_{i,j}, y_{i,j})$ is the local coordinate of ith vehicle at time $t_{i,j}$. $la_{i,j}$ is ID of the lane on which ith vehicle was at time $t_{i,j}$. $Pvid_{i,j}$ and $Fvid_{i,j}$ are the ID's of preceding vehicle and following vehicle of ith vehicle at time $t_{i,j}$, respectively.

Table 3.1 Structure of a NGSIM data set

Vehicle ID	**Time**	**Local X**	**Local Y**	**Lane ID**	**Preceding Vehicle**	**Following Vehicle**	**...**
vid_1	$t_{1,1}$	$x_{1,1}$	$y_{1,1}$	$la_{1,1}$	$Pvid_{1,1}$	$Fvid_{1,1}$	...
vid_1	$t_{1,2}$	$x_{1,2}$	$y_{1,2}$	$la_{1,2}$	$Pvid_{1,2}$	$Fvid_{1,2}$	...
...	...	...	...	...	...	...	...
vid_2	$t_{2,1}$	$x_{2,1}$	$y_{2,1}$	$la_{2,1}$	$Pvid_{2,1}$	$Fvid_{2,1}$	...
vid_2	$t_{2,2}$	$x_{2,2}$	$y_{2,2}$	$la_{2,2}$	$Pvid_{2,2}$	$Fvid_{2,2}$	...
...	...	...	...	...	...	...	...

3.2.1 Extraction of Lane Changing Information

By having this much information mentioned in section 3.2.1, it is possible to obtain a list of lane changing maneuvers in the aerial shooting area and period. In order to get this list we must first define an applicable definition for a lane changing maneuver.

- A Lane Changing Maneuver is an operation conducted by a vehicle's driver that changes this vehicle's trajectory from one lane to another.

According to this definition, we can extract lane changing maneuvers by comparing the lane ID column of every row entry with lane ID's from its adjacent rows. If a vehicle has different lane ID's from adjacent aerial shooting frames, we consider the definition of lane changing maneuver is met, and thus the corresponding vehicle ID and time stamp will be included into the lane changing maneuver list. So in order to extract the list of lane changing maneuvers, we only need vehicle ID, time, and lane ID.

The exact algorithm for finding lane changing maneuvers is shown in figure 3.6. Essentially this algorithm is executed by a nested loop. The outer layer loop execute inner layer loop, which finds lane changing maneuvers for a fixed vehicle, for every vehicle observed in a data set. The inner layer loop focus on one specific vehicle and examines all rows of record corresponding to this vehicle. Every row corresponds to one frame and has a time stamp, with all information entries in it. Usually adjacent rows come with adjacent time stamps, with a difference of shooting time at 1 mil-

lisecond. So we can compare lane ID's of adjacent rows for a decision of whether this vehicle changed its lane at a specific time. By doing this comparison for all available rows, we find a vehicle's all lane changing maneuvers and register them into a list, and then merging lists of all available vehicles in a recorded data set, an output of all lane changing maneuvers is produced.

In figure 3.6, i, j, are integers indicating number of loops executed, N is the number of vehicles recorded in a data set, M is the number of frames recorded for a specific vehicle, V is a vehicle's ID and $laneID$ is a laneID, LC is a list of lane changing maneuvers and its contained information includes vehicle ID, time stamp, and lane changing direction d, which is calculated by differentiating $laneID$'s before and after the maneuver. So when a vehicle changed its lane toward left, $d = -1$, and $d = 1$ means it changed toward right. Sometimes output of d are integers greater than 1, and we consider these situations as error, because under normal circumstances, it is not possible for a vehicle to move laterally further than a lane's width in 1 millisecond.

As the goal of this research is on patterns of drivers' decision making for lane changing, we need more information than merely a lane changing maneuver list. Potential information entries help a driver's decision include: global and local coordinates, speed, and acceleration. All these entries should be retrieved for the lane changing vehicle and its preceding vehicle, following vehicle, and vehicles longitudinally preceding and following the lane changing vehicle on neighbouring lanes.

Besides what is mentioned above, we also need the neighbouring vehicles' information. Related vehicles include: the lane changing vehicle's preceding vehicle, following vehicle, longitudinally preceding vehicle on right neighbour lane, longitudinally following vehicle on right neighbour lane, longitudinally preceding vehicle on left neighbour lane, and longitudinally following vehicle on left neighbour lane. So at most we can extract information for 6 neighbouring vehicles of the lane changing maneuverer. And by having all these neighbouring vehicles' locations, it is possible

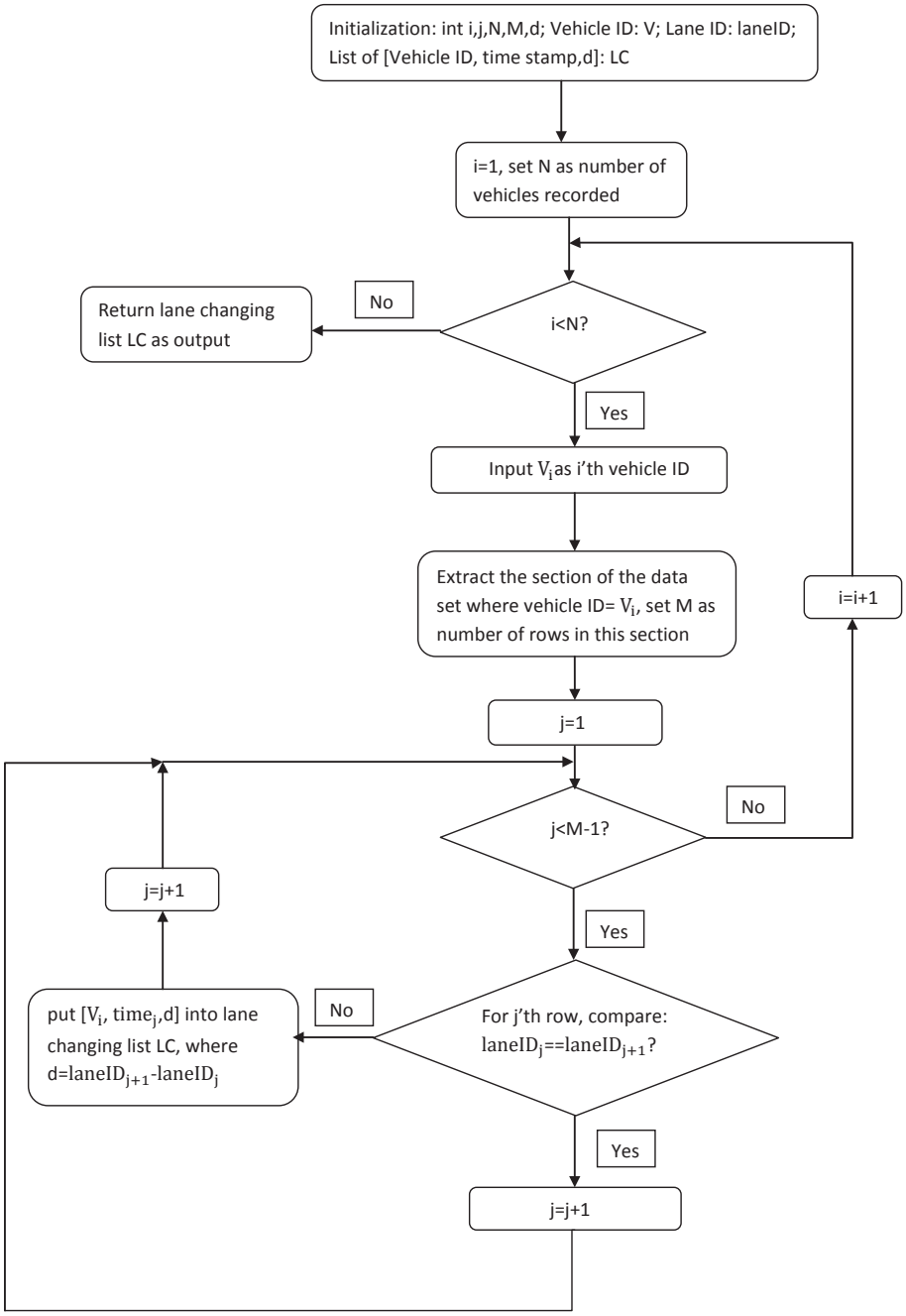

Figure 3.6 Algorithm for finding lane changing maneuvers in an NGSIM data set

to calculate gaps, relative speed, and relative acceleration etc. between any two of them. Also these pieces of information are not only collected at the time when the lane changing maneuver happened, we collect them for a short period before the maneuver was conducted, so we can analyze drivers' lane changing decisions, and answer questions include: under what does a driver decide to change his/her lane? What does a driver do right before lane changing? etc.

3.3 From Flow To Parameters: Principle of Calibration Methodology

3.3.1 Background

In this section we introduce how to use empirical flow data to determine average values of human factor parameters. Naturally his problem becomes a calibration problem of traffic flow models.

Generally speaking, calibration problems leads to optimization problems. However, under most circumstances people solve optimization problems by applying numeration methods, considering it's not easy to find a universal method for a kind of problems. So even successful commercial optimization packages, like IBM ILOG CPLEX Optimizer, work in an extremely time-consuming way. Meanwhile most root-finding problems have corresponding well-defined solving methods, either analytical or numerical, or both. And among these methods a lot are time-efficient, such as bisection method and Newton's method for solving linear equations, and Crank-Nicolson method for partial differential equations.

Based on facts mentioned above, we determine principle of this research as converting an optimization problem into a root finding problem. However the challenge here is, an optimization problem requires a solution which achieves the minimized value of its objective function, whilst what a root finding problem need is a solution to get value of a function equal to zero. So regarding this particular calibration

problem, we establish a function 3.19. And when value of this function goes towards zero, a traffic flow model gets better accuracy. In this way we convert an optimization problem into a root-finding problem, and then it's possible to apply numerical methods for solutions. Method of establishing this variable is introduced in section 3.3.4.2.

3.3.2 Essential Points of This Methodology

To achieve an approach for such a system, three requirements are pointed out:

1. This approach should be able to precisely reflect traffic conditions at the specific moment on a chosen segment of highway;

2. Computation should not be a significant burden so the system can react to changing situations immediately;

3. Algorithm adopted by this system must have a rigorous mathematical derivation of evaluating criterion.

Item 1 is intuitive since precision is fundamental for a research on calibration. In item 2, by emphasizing efficiency of the algorithm this system adopts, it's necessary to get it react quickly, and this fact further strengthen the system's ability to reflect real situation on assigned location and time. Also we design the third item because such a system is supposed to work in various environments, regardless of different traffic flow, density, speed, or such rates affected by abnormal situations.

To achieve these objectives, following ideas are raised:

1. Aggregating raw observation data to reduce the algorithm's running time, and applying coefficients on aggregated observation points to offset loss on accuracy because of data aggregation;

2. Using bisection method to reach a solution of optimized parameters rapidly.

3.3.3 An Introduction to Bisection Method

In engineering applications, there are usually complex computing tasks requires high amount of resources on both time and hardware. This leads to an obvious conflict between efficiency and cost. As a compromised solution, scientists in applied mathematics developed a series of algorithms to approximate solutions of specified computing problems. In this way an algorithm, which we call a numerical method, is designed to deliver an approximated solution to a computing problem with an high enough thus adjustable accuracy.

Among the most well-known numerical algorithms, bisection method, also known as binary search method, is widely used because of its simplicity and robustness. As most other numerical algorithms, this method is applied to solve root-finding problems $f(x) = 0$ where the continuous function f is defined on interval $[a, b]$ as sign of $f(a)$ is opposite to $f(b)$'s. Thus such a problem can be described as:

$$\begin{aligned} &f(x) = 0 \qquad x \in [a, b] \qquad a < b \\ &f(a) \times f(b) \leq 0 \end{aligned} \tag{3.9}$$

A loop is designed to solve the problem described in equation 3.9 that, in every iteration of the loop we divide the interval $[a, b]$ into two halves $[a, \frac{a+b}{2}]$ and $[\frac{a+b}{2}, b]$. By computing value of function f at midpoint $\frac{a+b}{2}$, we can determine which half of the interval a root of $f(x) = 0$ lies in. If $f(\frac{a+b}{2})$ has the same sign with $f(a)$ then there must be a root in interval $[\frac{a+b}{2}, b]$, or if $f(\frac{a+b}{2})$'s sign is also $f(b)$'s a root can be find in $[a, \frac{a+b}{2}]$. Also it's theoretically possible, but very unlikely, that $f(\frac{a+b}{2}) = 0$ which leads to an exact solution $\frac{a+b}{2}$. As this looping going, interval $[a, b]$ keeps shrinking and this method makes sure that there is a root lies in this interval. So when length of $[a, b]$ is smaller than expected error ϵ, either a or b can be final result of this looping as approximated solution to problem expressed in equation 3.9. This

means we can take $c = \frac{a+b}{2}$ as final result when length of $[a, b]$ is smaller than 2ϵ, since in this way one less loop is computed to get a better performance on running time. So determination of the result from this method can be described in equation 3.10, as s denotes approximated solution for above root-finding problem and ϵ is the maximum error allowed:

$$s = \frac{a+b}{2} \qquad when \quad |a-b| < \epsilon \tag{3.10}$$

Though there are many methods providing faster convergence, we still adopt bisection method instead of other options. And the reason is, our problem is finding root for a function defined in equation 3.19, and this function is not a definite mathematical function, so simplicity of a root finding method is essential to guarantee robustness under any possible situation of input data provided. For example, Newton's method is more advanced compared to bisection method but requires derivation operations, and in this case derivation leads to unpredictable results. After testing repeatedly, we see bisection method delivers both time efficiency and robustness we need.

And figure 3.7 shows principle of how this method works.

3.3.4 Structure of Algorithm

Structure of our methodology is a nested two level looping. The inner looping is a collection of evaluating results for a particular set of parameters of a traffic flow model, and the outer looping is an implementation of bisection method for search of a set of optimized parameter. And before the nested looping we aggregated data first.

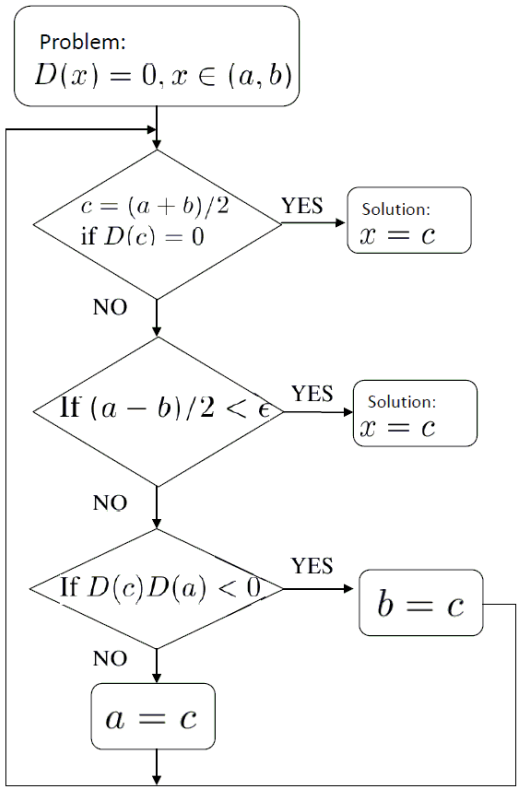

Figure 3.7 Flow chart for bisection method

3.3.4.1 Data Aggregation

To reduce running time of this algorithm, aggregation of empirical data should be the first step. We aggregate raw field observation data by averaging 3-D data values along an axis. For example, a set of speed-density-flow data are aggregated by averaging speed, density and flow values of all observations fall into a section $k^{(i)} < k < k^{(i+1)}$, where $k^{(i)}$ and $k^{(i+1)}$ are lower and upper bounds of ith density section. And this procession can be expressed as:

$$\bar{v}_i = \frac{1}{n}\sum_{j=1}^{n_i}(v_{ij})$$
$$\bar{k}_i = \frac{1}{n}\sum_{j=1}^{n_i}(k_{ij})$$
$$\bar{q}_i = \frac{1}{n}\sum_{j=1}^{n_i}(q_{ij}) \tag{3.11}$$

where footnote i means this calculation is for ith density slice, n_i is number of raw observations in this slice, $\bar{v}_i$, $\bar{k}_i$ and $\bar{q}_i$ are averaged values of v, k and q for ith slice, respectively. v_{ij}, k_{ij} and q_{ij} are coordinates for jth raw observation in ith slice of v-k-q coordinate system.

3.3.4.2 Inner Looping: Evaluation of Parameters

3.3.4.2.1 Derivation of Objective Function A calibration criterion has been raised by H. Rakha and M. Arafesh Rakha & Arafeh (2010) is formulated as:

$$Min \quad E = \sum_i \left\{ \left(\frac{v_i - \hat{v_i}}{\tilde{v}} \right)^2 + \left(\frac{q_i - \hat{q}_i}{\tilde{q}} \right)^2 + \left(\frac{k_i - \hat{k_i}}{\tilde{k}} \right)^2 \right\} \tag{3.12}$$

where q_i, k_i and v_i are flow, density and average speed data from field tests, respectively. $\hat{q}$, $\hat{k}$ and $\hat{v}$ are flow, density and average speed derived from a model, as $\tilde{q}$, $\tilde{k}$ and $\tilde{v}$ are maximum value of flow, density and speed observed in filed. This is a very good estimation for models simulating traffic flows, however, two concerns still worth more research for solutions:

1. There is still room for improvement on time and resource efficiency. It's acceptable to compromise on accuracy of an algorithm in order to get it faster.

2. All aggregated data dots receive the same treatment, while in fact some of the dots are aggregated from more raw field observations than others, as there are

many more vehicles travelling around 60 mph than those opt 30 mph on the same section of highway;

Regarding issue 1, since $q_i = k_i \times v_i$, also approximately $\hat{q_i} \approx \hat{k_i} \times \hat{v_i}$ and $\tilde{q_i} \approx \tilde{k_i} \times \tilde{v_i}$, thus we consider flow q in this evaluation criterion redundant, which means we can get the same result by switching to criterion 3.13 instead of 3.12:

$$Min \quad E = \sum_i \left\{ \left(\frac{v_i - \hat{v_i}}{\tilde{v}} \right)^2 + \left(\frac{k_i - \hat{k_i}}{\tilde{k}} \right)^2 \right\} \tag{3.13}$$

As shown in section 3.3.4.1, we make narrow slices on k-v coordinate system to get groups of data for aggregation, and here we presume it's k-axis we slice to group data, so each observation falls into ith group satisfies $k^{(i)} < k \leq k^{(i+1)}$, where $k^{(i)}$ and $k^{(i+1)}$ are lower and upper bounds of ith density section. According to equation 3.11, we get aggregated dot's coordinate on k-axis by averaging all raw observations' corresponding coordinates, thus if we opt middle point between $k^{(i+1)}$ and $k^{(i)}$, instead of $\bar{k_i}$, to approach k_i the corresponding error would be:

$$\begin{aligned} & err \leq \frac{\epsilon}{2} \\ & \epsilon = k^{(i+1)} - k^{(i)} \\ & when \quad k_i = \frac{k^{(i+1)} + k^{(i)}}{2} \end{aligned} \tag{3.14}$$

where err is error derived from approximation for k_i by middling ith slice and ϵ is width of ith slice. So obviously if we set ϵ to be a small enough number it's possible to opt equation 3.14 as approximation for k_i without losing too much accuracy. In our simulation we choose $\epsilon = 0.5$ vehicle/km. In this way we avoid calculating average value of a set of observations as shown in equation 3.11.

By narrowing slices on k-axis, another obvious strategy is intuitive that, in calculation for equation 3.13 we can ignore the second term which is square of relative difference for density k. This is because in a slice, relative difference between densities of a raw observation and the aggregated dot is very small, especially compared to that between speeds of the same dots. This can be proved by computing curve of the following function 3.15, which is relationship between two terms in equation 3.13:

$$f = \frac{\sum_i \left(\frac{v_i - \hat{v_i}}{\tilde{v}}\right)^2}{\sum_i \left(\frac{k_i - \hat{k_i}}{\tilde{k}}\right)^2} \tag{3.15}$$

This curve is shown in figure 3.8. Also this figure perfectly explains drivers' different behaviour patterns corresponding to different density rates. When density is very low (lower than 7 vehicles per km), drivers opt different speeds freely according to their own preferences, so speeds under such situations are distributed widely because of big variance on people's personal preferences. When there are some more vehicles on road but still not too many (8 to 24 vehicles per km), traffic flows travel fast, so under such circumstances drivers who prefer driving slowly are encouraged to drive faster to follow the flow. And as density grow higher to around 40 vehicles per km, average speed decreases remarkably. Actually average speed at this stage is so low that a significant proportion of drivers opt fast lanes for higher speed and overtaking, and this causes a peak at 40 vehicles per km. As density goes up, there is less room for drivers' maneuvers including lane-changing, accelerating and braking, thus there are less people driving aggressively, and this makes the curve going down gradually at density higher than 40 vehicles per km.

Thus we can delete second term in criterion 3.13 without losing too much on precision of a model. In this way we improve it into equation 3.16:

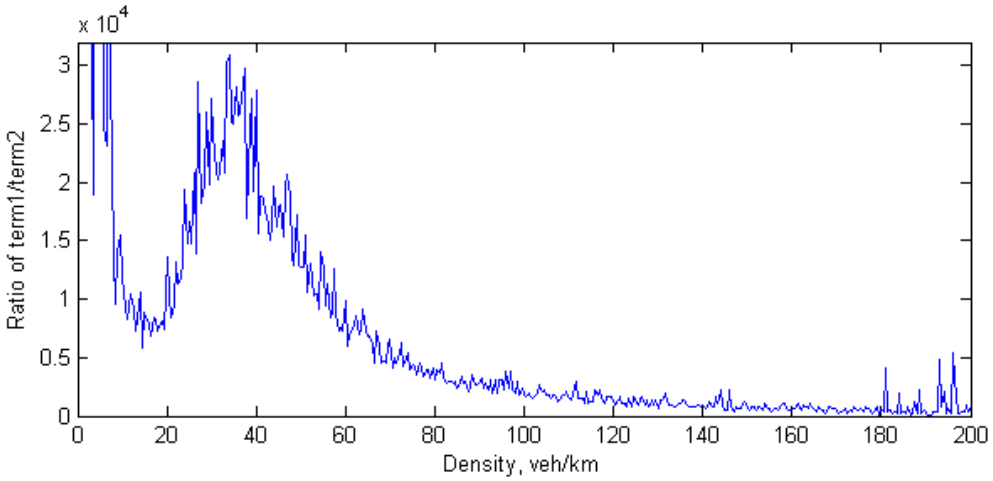

Figure 3.8 Curve computed from function 3.15

$$Min \quad E = \sum_i \left(\frac{v_i - \hat{v_i}}{\tilde{v}} \right)^2 \tag{3.16}$$

Actually here we don't need the denominator $\tilde{v}$, as for a optimization problem, dividing its objective function by a constant doesn't make any difference to the result. Similarly, replacing square operation by calculating absolute value won't affect optimization result since minimizing an equation's square leads to the same point of that by minimizing its absolute value . Thus equation 3.17 reflects exactly the same criterion with equation 3.16.

$$Min \quad E = \sum_i |v_i - \hat{v_i}| \tag{3.17}$$

Here v_i is speed value for an aggregated field observation, and $\hat{v_i}$ is the estimated speed corresponds to density value of the same aggregated observation. This estimation of speed is done by applying macroscopic traffic flow simulation models.

By opting equation 3.17 as objective function, it's convenient to calculate its value without any other looping. Whilst Rakda's method with objective function 3.12

requires another level of optimization to find a point (q_i',k_i',v_i') which is the nearest one on a curve to an aggregated observation (q_i,k_i,v_i). Usually this kind of optimization uses a looping to try a series of points on the curve, after calculating distance from every of this series of points to the observation(q_i,k_i,v_i), point with the least distance is considered as nearest point from the curve to (q_i,k_i,v_i). In our algorithm this level of optimization can be avoided, thus a considerable amount of time is saved from this step.

3.3.4.2.2 Conversion to A Root-Finding Problem In order to implement bisection method in later section 3.3.4.3, it's necessary to convert this optimization problem into a root-finding problem. Key to this conversion is finding a function which has a root in a domain of its parameters, and such a root should be very near, if not the same, to solution of the optimization problem solved with objective function 3.17. Thus, we assign positive and negative signs to results of inner looping. In the case discussed above, if an aggregated observation point locates at left side of corresponding speed-density curve we multiply the result of its objective function by -1, and if it sits at right side then keep it as positive. Actually This strategy can be applied simply by removing absolute value calculation in objective function 3.17. So the root-finding problem is as following function 3.18.

$$F = \sum_i v_i - \hat{v_i} \tag{3.18}$$

In this function every aggregated observation are considered equally important, however, in reality we don't agree with this assumption, since during most time vehicles travel in traffic with density less than 50 vehicles per km. Our observation data reveals that more than 60% traffic happens with density lower than 50 vehicles per km, and this can be found in following figure 3.9.

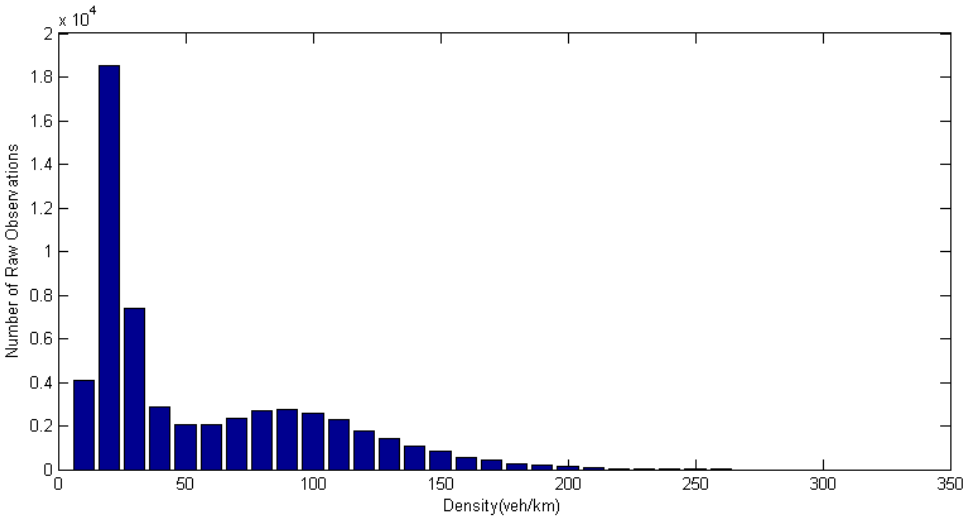

Figure 3.9 Number of raw observations happened at different density levels

So it's appropriate to multiply every aggregated observation with a term of weight which is number of raw observations it's aggregated from. So we have the final version of the root-finding problem as function 3.19.

$$F = \sum_i n_i(v_i - \hat{v}_i) \tag{3.19}$$

where n_i is the number of raw observations fall into ith slice of k-v plane, and these raw observations are used to produce ith aggregated observation by applying equation 3.11. Here we name result of this function as Degree of Satisfaction for a set of parameters, and purpose of inner looping is to find degree of satisfaction for a specific set of parameters whilst outer looping explained in section 3.3.4.3 is to find a set of parameters which has its degree of satisfaction the nearest one to zero.

3.3.4.3 Outer Looping: Bisection Method

As we get degree of satisfaction of every set of parameters in inner looping, different parameter sets get evaluated by running outer looping. Goal of this evaluation is to find a set of model parameters which let right side of equation 3.19 equals to 0. So

the problem here is to find a root for this function, and intuitively numerical analysis methods can help because it's not a simple linear function. Here we adopt bisection method because of its simplicity and robustness. Using LCM model as an example to calibrate:

$$k = \frac{1}{(\gamma v^2 + \tau v + l)[1 - \ln(1 - \frac{v}{v_f})]} \tag{3.20}$$

where k is traffic density, v is space-mean speed, γ denotes aggressiveness that characterizes the driving population, τ average response time that characterizes the driving population, l average effective vehicle length, and v_f free flow speed. So in this model we need to allocate four parameters γ, τ, l and vf. As an example, steps of this bisection algorithm to optimize γ include:

- Step 1 If any of τ, l and v_f has already been optimized before γ, set these parameters as their calibrated values. And for those have not been calibrated, set default parameter values. Default values are best guesses based on common sense and earlier experience. For γ we set lower bound γ_l and upper bound γ_u. Set acceptable largest error of gamma ϵ.

- Step 2 If $\gamma_u - \gamma_l < \epsilon$ then return $\gamma = (\gamma_l + \gamma_u)/2$ as result of this algorithm, and quit algorithm. Otherwise, run inner looping with $\gamma = (\gamma_l + \gamma_u)/2$ and other parameter values as set in step 1 for LCM model, get degree of satisfaction for this set of parameters with new γ value.

- Step 3 If degree of satisfaction value got in step 2 is greater than 0, it means we underestimated drivers' aggression at this particular time and location, thus reset lower bound of aggressiveness as $\gamma_l = (\gamma_l + \gamma_u)/2$, keep other parameters unchanged and go to step 2. Otherwise it means we overestimated drivers' aggressiveness so reset upper bound as $\gamma_u = (\gamma_l + \gamma_u)/2$ and go to step 2.

With this bisection algorithm we will finally get a calibrated γ value when sum of signed distances is very near to 0, which means our calibration criterion is approximately satisfied. And repeat this for every model parameter.

3.4 From Human Factor Parameters to Flow: Principles of Transformations Between Distributions

Though the previous section 2.3 presented a set of mathematical models to capture the effect of P-R time on flow and capacity, two limitations have to be noted. First, these models are formulated assuming regular traffic where human drivers take full control over their vehicles without receiving assistance from connected vehicle technology. Second, these models are essentially deterministic assuming a constant P-R time for each driver. In this research, our goal is to understand how flow and capacity would change if drivers are assisted by connected vehicle technology so that their P-R times are enhanced. Therefore, the above models alone are insufficient to serve our purpose because we need a mechanism to incorporate the enhancement on P-R time and its randomness and to factor them in the resultant flow and capacity.

Our approach is statistical transformation. More specifically, we consider P-R time τ as a random variable which follows a distribution. As such, it is possible to transform the distribution of τ into the distribution of traffic flow rate. In order to accomplish this transformation, we need to first find out how to transform a random variable distribution into another.

Any function of the random variable P-R time τ, $g(\tau)$, is also a random variable Casella & Berger (2001). Taking flow rate X as an example, intuitively we want to describe random variable $X = g(\tau)$ with a distribution. Thus it's convenient to describe probabilistic behaviour of X in terms of that of τ, as X is a function of τ. That is, for any set A,

$$P(X \in A) = P(g(\tau) \in A) \tag{3.21}$$

So the distribution of X is defined by function g and τ's p.d.f. (probability density function) f_τ. Thus it's possible to derive an expression of X's p.d.f. f_X assuming some properties of function g. The definition of $x = g(\tau)$ as a function of random variable τ is the following: $g(\tau)$ defines a mapping from $\mathcal{T}$ (the original sample space of τ) to $\mathcal{X}$ (the sampling space of flow rate X). Or we can express it as:

$$g(x) : \mathcal{T} \longrightarrow \mathcal{X} \tag{3.22}$$

Thus the inverse function of g is an inverse mapping of the above, denoted by g^{-1}. This is a mapping from subsets of $\mathcal{X}$ to subsets of $\mathcal{T}$, with its definition:

$$g^{-1}(Y) = \{\tau \in \mathcal{T} : g(\tau) \in Y\} \tag{3.23}$$

where Y is a subset of $\mathcal{X}$. So this g^{-1} maps one set into another. More precisely, g^{-1} is a set of elements in $\mathcal{X}$ which $g(x)$ maps into set Y. And of course for a single element of x, we can set a point set $Y = \{x\}$, thus in this way, definition of g^{-1} in equation 3.23 solves any possible situation of X. And for the point set case, we write it as $g^{-1}(x)$ for convenience. Another point worth being mentioned is that, it's possible to find more than one values of x for which $g(\tau) = x$, so $g^{-1}(x)$ can be a set of different values of τ. Or if there is only one value of τ satisfy $g(\tau) = x$, we write $g^{-1}(x) = \tau$ as g^{-1} is a point set $\{\tau\}$.

$$g^{-1}(x) = \tau \qquad \tau \in \mathcal{T}, g(\tau) = x \tag{3.24}$$

By defining random variable X as $X = g(\tau)$, for any set $Y \subset \mathcal{X}$,

$$\begin{aligned} P(X \in Y) &= P(g(\tau) \in Y) \\ &= P(\tau \in \mathcal{T} : g(\tau) = Y) \\ &= P(\tau \in g^{-1}(Y)) \end{aligned} \tag{3.25}$$

where operator P is the probability of its input, and obviously $0 < P < 1$. Equation 3.25 defines the distribution of X's probability. To justify this definition of probability distribution, we test it with Kolmogorov Axioms below:

$$\begin{aligned} &P(E) \in \mathbb{R}, P(E) \geq 0 \qquad\qquad \forall E \in F \\ &P(\Omega) = 1 \\ &P(E_1 \cup E_2 \cup E_3 \cup \dots) = \sum_{i=1}^{\infty} E_i \end{aligned} \tag{3.26}$$

where F is the event space and E is any event in F. Ω stands for the fact that some elementary event in the entire sample space will occur. $E_1, E_2, \dots$ are disjoint events in space F. For the first clause of the Kolmogorov Axioms, for any possible X, it's straightforward that the corresponding $P(\tau \in g^{-1}(Y))$ is greater than or equal to 0, as it's a probability. For the second clause, sum of all $P(X \in Y)$ corresponding to τ's those satisfying $P(\tau \in g^{-1}(Y)) > 0$ is 1, as all such τ's constitute the set $g^{-1}(Y)$. And probability for any other τ's outside $g^{-1}(Y)$ is 0, so clause 2 of Kolmogorov

Axioms is satisfied. Also as all events in this case are mutually exclusive, clause 3 is obviously satisfied.

In order to keep track of sample spaces of random variables, which in our case are P-R time and flow rate, we define them for transformation $X = g(\tau)$ as:

$$\begin{aligned} \mathcal{T} &= \{\tau : f_\tau(\tau) > 0\} \\ \mathcal{X} &= \{x : x = g(\tau) \quad for\ all\ \tau \in \mathcal{T}\} \end{aligned} \tag{3.27}$$

These are support sets of distributions of random variables τ and flow rate X, as p.d.f. of a random variable is positive only on the corresponding set and is 0 elsewhere.

By the nature of relationship between P-R time τ and flow rate X, function $g(\tau)$ is monotone, or more precisely, increasing. That is,

$$\tau_1 > \tau_2 \quad \Rightarrow \quad g(\tau_1) > g(\tau_2) \tag{3.28}$$

This property of the function will make our work on transforming much easier, as a monotone transformation $\tau \to g(\tau)$ implies that the mapping from $\mathcal{T}$ to $\mathcal{X}$ is one-to-one. Also as defined in equation 3.27, for each $x \in \mathcal{X}$ there is a τ such that $g(\tau) = x$, thus this function is an onto one. So function $x = g(\tau)$ is one-to-one and onto. Thus this transformation maps τ's to x's uniquely. As g is monotone and increasing, we get $g^{-}1$ single-valued. Thus,

$$\begin{aligned} \{\tau \in \mathcal{T} : g(\tau) < x\} &= \{\tau \in \mathcal{T} : g^{-1}(g(\tau)) \leq g^{-1}(x)\} \\ &= \{\tau \in \mathcal{T} : \tau \leq g^{-1}(x)\} \end{aligned} \tag{3.29}$$

In order to better deriving a transformation rule, we define and derive c.d.f. (cumulative density function) of the random variable X as below:

$$\begin{aligned} F_X(x) &= P(X \leq x) \\ &= P(g(\tau) \leq x) \\ &= P(\{\tau \in \mathcal{T} : g(\tau) \leq x\}) \\ &= \int_{\{\tau \in \mathcal{T} : g(\tau) \leq x\}} f_\tau(\tau) d\tau \end{aligned} \tag{3.30}$$

Here we assume both random variables τ and X are continuous, and this is true in the case of P-R time and flow rate. By combining equations 3.29 and 3.30, we get:

$$\begin{aligned} F_X(x) &= \int_{\{\tau \in \mathcal{T} : g(\tau) \leq x\}} f_\tau(\tau) d\tau \\ &= \int_{-\infty}^{g^{-1}(x)} f_\tau(\tau) d\tau \\ &= F_\tau(g^{-1}(x))) \end{aligned} \tag{3.31}$$

As we defined before, F_X and F_τ are c.d.f.'s of random variables X and τ, while f_X and f_τ are p.d.f.'s of X and τ, respectively. And by taking a first order derivative of $F_X(x)$ with respect to x, we get

$$\begin{aligned} f_X(x) &= \frac{d}{dx} F_X(x) \\ &= f_\tau(g^{-1}(x)) \times \frac{d}{dx} g^{-1}(x) \end{aligned} \tag{3.32}$$

Thus we get the fundamental rule of transformation between two related distributions. Actually restriction for this rule is quite strong as in our case g is an increasing function, and a similar form of this rule works for a decreasing g as we need to add a term of -1 to the right hand side of equation 3.32. So a universal version of the fundamental rule is shown below:

$$f_X(x) = f_\tau(g^{-1}(x)) \times |\frac{d}{dx} g^{-1}(x)| \tag{3.33}$$

CHAPTER 4

RESULTS AND FURTHER ANALYSIS

4.1 Lane Changing Maneuver Information Extracted From NGSIM Data

As an example of using extracted information from NGSIM data, we demonstrate a simple lane changing model and calibrate it with the lane changing maneuver list obtained in chapter 3.2.1.

Taking the data set for Interstate 80 in Emeryville CA, collected between 8:20 am and 8:35 am, as an example. We extract all lane changing maneuvers satisfying two criteria: 1. difference between the vehicle's lane ID's before and after the maneuver is 1 or -1; 2. a record of at least 60 seconds right before the maneuver exists. In this case we extract out 66 maneuver records, of which 48 are toward left and 18 are toward right. So we focus on left shifts because of its greater sample size.

In our common sense, drivers execute lane changing maneuvers toward left because they want to drive faster than the traffic on their current lanes. So this means a lane changing driver has a higher demanded speed than his/her preceding vehicle's current speed. Here we assume that, at 1 minute before shifting to the left lane, a lane changing vehicle moves at its demanded speed. So a normal procedure of lane changing includes:

- The vehicle moves at its demanded speed, at 1 minute before its lane changing maneuver.
- The vehicle catches up a slow preceding vehicle it has to slow down.

- The driver decides to change lane, so accelerates and shifts left.

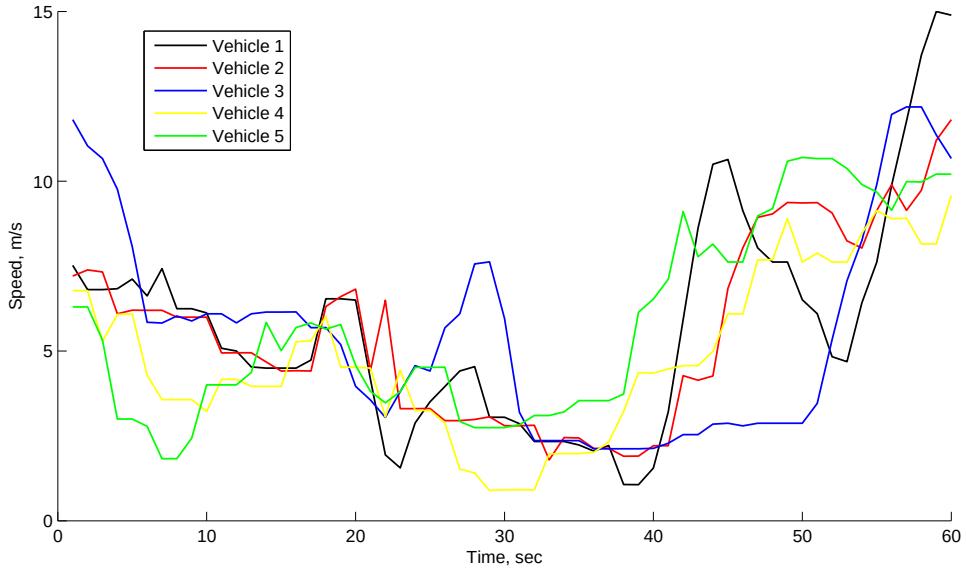

Figure 4.1 Speed profiles of vehicles in 60 second period before lane changing maneuver

This process can be observed in figure 4.1, which shows a random sample of left shifting vehicles' speed profiles for a period of 60 seconds before their lane changing maneuvers. Entering this 60-second period with an entry speed, these vehicles moved in a decelerating trend in the first 30 seconds, and reached the bottom of their speed between 30th and 40th seconds, where we name as developed speed. 20 seconds right before their lane changing maneuvers, vehicles accelerated at significant paces to shift to faster lanes at a speed named overtake speed.

So it is possible to model lane changing maneuvers by mathematically defining this pattern. We have the following definition for the pattern:

$$
\begin{aligned}
v_{entry} &= mean(v(1:5)) \\
v_{dev} &= min(v(31:35)) \\
v_{overtake} &= max(v(58:60)) \\
v_{dev} &< a \times v_{entry} \\
v_{overtake} &> b \times v_{entry}
\end{aligned} \tag{4.1}
$$

where array v is speed record for a 1 minute period in prior to the lane changing maneuver, with a sampling frequency of 1Hz, and thus array v has a length of 60. Method of obtaining this record is introduced in chapter 3.2.1. Functions $mean()$, $min()$, and $max()$ are self-explanatory. v_{entry} is entry speed of the lane changing vehicle while entering this 60 seconds period, v_{dev} is the developed speed defined between 31 and 35 seconds, and $v_{overtake}$ is the overtake speed at which the lane changing vehicle shifts to left lane and pass the slow preceding vehicle. a and b are coefficients to quantify the relationships between v_{entry}, v_{dev}, and $v_{overtake}$. So it's possible to check accuracies of different values for a and b on matching field data extracted from NGSIM. Table 4.1 shows numbers of recoded lane changing maneuvers satisfy rule 4.1 with specified values for a and b. Total number of lane changing maneuvers towards left in this case is 48.

So number of lane changing maneuvers satisfying rule 4.1 decreases as coefficient a decreases and coefficient b increases. This meets nature of the rule, as it seeks speed profiles lower in middle and higher in the end, and a smaller a and a greater b sets a more strict selecting criterion.

On the other hand, we can consider gaps as the main parameter in lane changing patterns.

Table 4.1 Number of record matches for different values of a and b

		a								
		1	**0.95**	**0.90**	**0.85**	**0.80**	**0.75**	**0.70**	**0.65**	**0.60**
b	**1**	31	31	30	28	26	26	22	22	20
	1.05	30	30	29	27	25	25	22	22	20
	1.10	29	29	28	26	25	25	22	22	20
	1.15	28	28	27	25	24	24	22	22	20
	1.20	25	25	24	22	22	22	20	20	18
	1.25	23	23	22	20	20	20	18	18	17
	1.30	23	23	22	20	20	20	18	18	17
	1.35	23	23	22	20	20	20	18	18	17
	1.40	22	22	21	19	19	19	17	17	16

$$g = \int_0^t (v - v_p)dt \tag{4.2}$$

As shown in equation 4.2, where g is gap, v and v_p are speeds of lane changing vehicle and its preceding vehicle, respectively, gap is simply a result of integrating difference between speeds of two vehicles. We suppose a lane changing vehicle's headway gap profile should have a pattern reflecting pattern of its speed profile. Based on the assumption that the preceding vehicle keep a stable lower speed, value of gap should have a descending profile, with a higher absolute value of its first order derivative at two ends, but lower at middle. However, field data doesn't shown this pattern, as shown in figure 4.2.

Figure 4.2 visualizes gap profiles of the same 5 randomly selected lane changing vehicles as in figure 4.1. In figure 4.1 these 5 vehicles' speed profiles show a clear pattern of descending and then ascending, however in figure 4.2 there is no such obvious pattern, except that the gap fluctuates dramatically in the final 20 seconds. This can be explained that, our previous assumption that the preceding vehicle keeps a stable speed was not satisfied. So when both lane changing vehicle and its preceding vehicle move at fluctuating speeds, the gap between them fluctuates even more dramati-

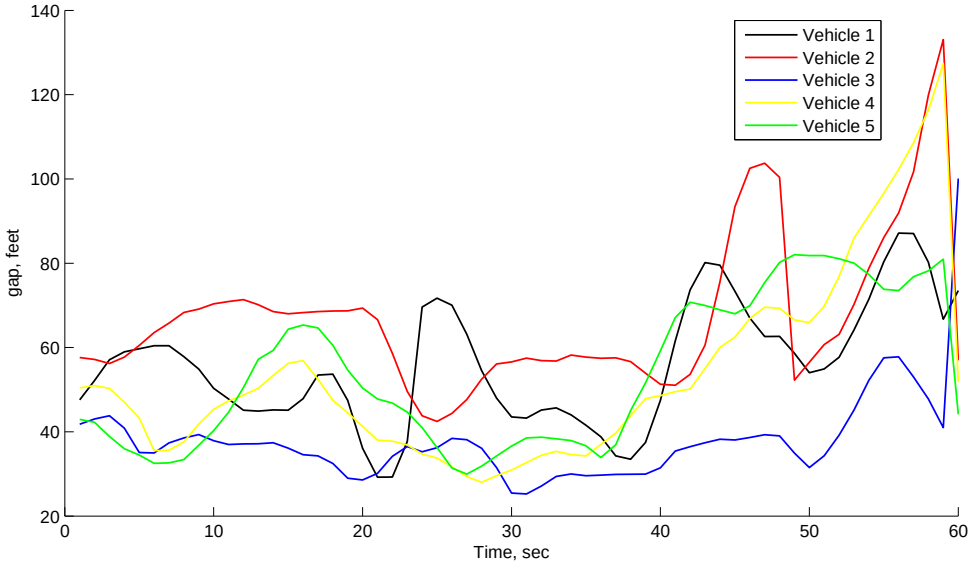

Figure 4.2 Gap profiles of vehicles in 60 second period before lane changing maneuver

cally but shows no pattern. This reasoning can be proved by figure 4.3, which shows profiles of relative speeds between lane changing vehicles and corresponding preceding vehicles. No obvious pattern is shown in these profiles except more dramatical fluctuations.

4.2 Impact of P-R Time Enhancement on Traffic Flow

Obviously when other aspects of the environment are kept the same, a driver assisted by connected vehicle technology can drive faster or closer to the front car if the driver necessitates shorter P-R time. If this holds true for all vehicles, a higher flow would result on the same roadway facility. In order to quantify the relationship between flow and P-R time, we utilize the p.d.f. transformation rule derived in the previous section. For illustration purpose, a normal distribution is assumed here as the underlying distribution of P-R time per findings of many human factors studies. Here, we limit our attention to 100% penetration of connected vehicles for two reasons. First, this is the goal of future transportation systems, so it makes practical sense to

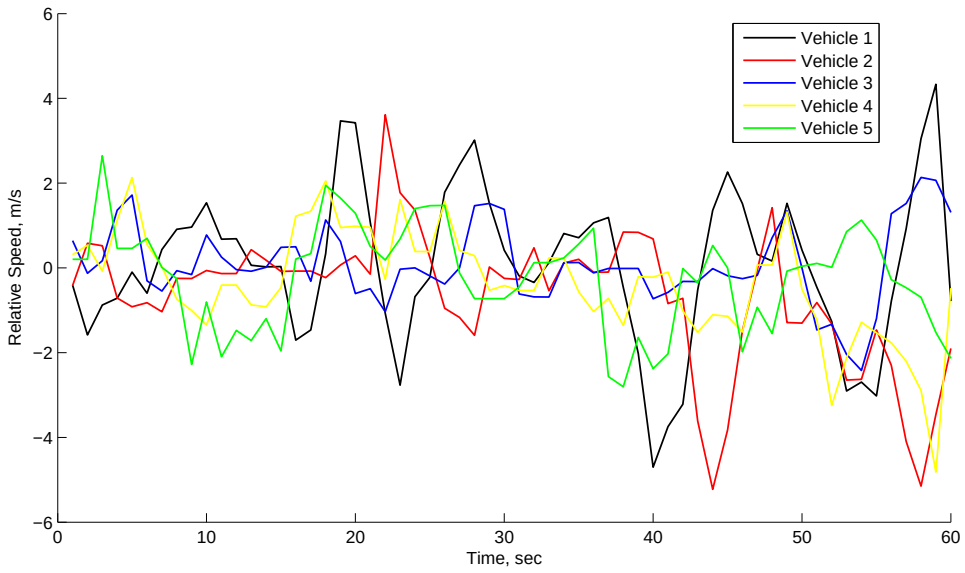

Figure 4.3 Profiles of relative speeds between lane changing vehicles and corresponding preceding vehicles in 60 second period before lane changing maneuver

focus on it first. Second, 100% penetration ensures that samples of P-R times come from the same population so that they are more likely to be normally distributed.

Notice that the transformation rule in equation 3.33 requires that function g be monotone, which is the case for the three models. Their inverse functions with respect to τ are:

Forbes model:

$$\tau = g^{-1}(q) = \frac{1}{q} - \frac{l}{v} \tag{4.3}$$

Simplified Gipps model:

$$\tau = g^{-1}(q) = \frac{1}{q} - \gamma v - \frac{l}{v} \tag{4.4}$$

LCM:

$$\tau = g^{-1}(q) = \frac{1}{q[1 - \ln(1 - \frac{v}{v_f})]} - \gamma v - \frac{l}{v} \tag{4.5}$$

Since the three inverse functions are similar in nature and the application of transformation rule follows the same procedure, we choose the simplified Gipps model for further discussion since this model is widely implemented in the community.

Inserting above g^{-1} expression into equation 3.33, we obtain the distribution of flow:

$$\begin{aligned} f_Q(q) &= f_\tau(g^{-1}(q)) \times |\frac{d}{dq} g^{-1}(q)| \\ &= \frac{1}{q^2} \frac{1}{\sigma\sqrt{2\pi}} e^{[-(\frac{1}{2\sigma^2})(\frac{1}{q} - \gamma v - \frac{l}{v} - \mu)^2]} \end{aligned} \tag{4.6}$$

As this is a probability distribution function, its value is always greater than zero even for $q < 0$. However, with possible values of μ and σ, cumulative value of probability for $q < 0$ is very small, normally less than 0.001. Thus we use this p.d.f. to approximate real p.d.f. of flow. An advantage of this model for predicting flow improvement is that, one only needs to measure changes in P-R time for parameters μ and σ, while other parameters are constant for a certain situation. For example, on a given segment of highway, both the segment's geometrical characteristics and its corresponding driver population are consistent over decades, so most parameters in the model can be calibrated through observed experiences. If P-R time enhancement by connected vehicle technology holds true, μ and σ may change dramatically, and thus this model can be used the evaluate the corresponding impacts. In this research, we adopt a Monte Carlo method for the evaluation purpose. Two scenarios are set up:

1. Normal traffic flow without P-R time enhancement. Drivers' average P-R time is 1.5 second, and corresponding standard deviation 0.5.

2. Traffic flow with average P-R time enhanced by connected vehicle technology. Average P-R time is enhanced by 10%, 20%, 30% and corresponding standard deviation is 0.4, 0.3, 0.2.

The procedure of the Monte Carlo method is the following:

1. Randomly sample 100 drivers' P-R time for each scenario with corresponding expectation and standard deviation. Then calculate mean and variance of the two sets of P-R times, the mean will be μ value for the simulation, and the variance will be σ^2.

2. For both cases, insert the simulated μ and σ into the p.d.f. of flow in Equation (4.6), with all other factors calibrated from observed experiences under normal circumstances, get two distributions, and visualize them.

3. Calculate the expectation and standard deviation of flow with the following equations:

$$
\begin{aligned}
E_q &= \int_0^\infty q f_Q dq = \int_0^\infty \frac{1}{q} \frac{1}{\sigma\sqrt{2\pi}} e^{[-(\frac{1}{2\sigma^2})(\frac{1}{q}-\gamma v-\frac{l}{v}-\mu)^2]} dq \\
\sigma_q^2 &= \int_0^\infty (q-E_q)^2 f_Q dq = \int_0^\infty (q-E_q)^2 \frac{1}{q^2} \frac{1}{\sigma\sqrt{2\pi}} e^{[-(\frac{1}{2\sigma^2})(\frac{1}{q}-\gamma v-\frac{l}{v}-\mu)^2]} dq
\end{aligned}
\tag{4.7}
$$

Simulated result of the p.d.f. of flow under these two scenarios are shown in Figure 4.4 and Table 4.2 lists properties of P-R time samples and flow distributions. Note that these distributions were calculated under assumptions that $v_f = 96$ km/h and v

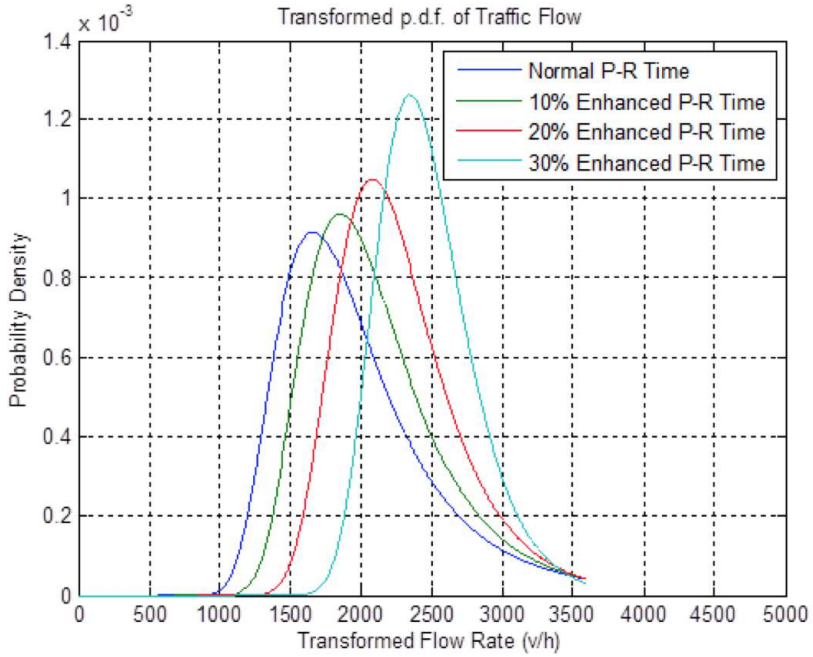

Figure 4.4 Comparison of the distributions of flow

Table 4.2 One set of simulation results for two scenarios

Scenario	**Mean of P-R time**	**Std of P-R time**	**Mean of Flow**	**St.d. of Flow**
P-R not enhanced	1.50	0.50	1885	488
P-R enhanced 10%	1.35	0.40	2035	456
P-R enhanced 20%	1.20	0.30	2216	407
P-R enhanced 30%	1.05	0.20	2447	332

= 90 km/h. Bear in mind that the result is meant to provide an illustrative example and analysts can follow the same procedure to calibrate to their specific problems.

In Figure 4.4 it is obvious that the flow with enhanced P-R time has increased compared to that without enhancement. The enhanced flow has a larger mean and a smaller variance, which suggests that P-R time enhancement by connected vehicle technology can potentially improve traffic flow to a higher and more consistent level without modifying existing facilities. In addition, the result in Table 4.2 reveals that, as the mean of flow increases, the standard deviation of flow drops.

An intuitive explanation for this phenomenon is that, as the average P-R time of a driver population is enhanced, drivers are able to follow their leading vehicles closer than before without having to reduce speed. At the same speed, shorter average gap means higher density which in turn translates to increased flow.

Note that, though the above study is based on the chosen modes and distributions, the methodology is generic and accommodates other models and distributions. In addition, the numerical and simulation results are for illustration purpose, and analysts need to customize and calibrate the methodology including the underlying models and distributions to the specific problem under study for accurate results.

4.3 From Flow to Human Factor Parameters: Calibration Results and Analysis

To verify and analyse approach introduced in chapters 3.3 and 3.3.4, we pick eight sample sets of 5 minute traffic data to verify and analyse our algorithm. These samples are cut from a set of traffic flow data logs for route 400 in Georgia in July 2003, contain information collected by two roadside cameras. Four of the 5 minute samples derived from logs collected by camera 1106 near North Old Milton Parkway, Alpharetta, GA (Location A), and the other four are related to logs of camera 1134 near South Hammond Drive, Sandy Springs, GA (Location B). These traffic data logs

contain raw observations of flow, density and speed with time stamps. Every raw observation was for a 20 seconds period, so information contained by an observation is average rate of flow, density, speed of traffic went through a camera's shooting area during a specific 20 second period. Thus this data set is capable to simulate traffic situation in real time except one fact that, size of data log in reality would be much bigger than our data set since we assume real time data stream are observations for individual vehicles, not averaged traffic during periods. To solve this problem we aggregate data from logs of different days in July into one sample. For example, in order to get a sample for traffic during 9:00-9:05 am at camera 1106, we aggregate all traffic data for this site and this time of day on all days in July into one single file as a simulation of real time observation of individual vehicles. Since traffic flow characters should be consistent for the same site under the same illumination, it's reasonable to simulate by aggregating.

In order to get samples without any preference, for each site we pick four 5 minute segments of the logs with a 3 hour step, that is, these four samples are log segments of traffic data at 9:00-9:05 am, 12:00-12:05 pm, 3:00-3:05 pm and 6:00-6:05 pm respectively.

4.3.1 Data Aggregation and Weighting

As the first step, data aggregation contribute remarkably for saving running time. 150 slices on k-axis are made on interval $k \in [0,300]$, however, consider there are slices where there are no raw observation fall in, actual number of aggregated observation points is less than 150. As shown in figure 4.5, there are 15-70 aggregated points depends on span of raw data's density value. Also from this figure we see obvious patterns of traffic flow in different time of a day. In the morning majority of traffic travelled at density $k < 30$ vehicles per km, higher density happened sometimes and were not ignorable, especially for camera 1134 at location B. This is just the nor-

mal situation on highway, sequences of vehicles come with considerable high internal density but there are long distances between different sequences. And sometimes slow leading vehicles of sequences make traffic slow down. During noon time traffic was more concentrated to density under 30, sparse points exist at higher density and lower speed, so it's still normal situation with minor differences. Traffic situation in afternoon were significantly different. For sample data at 3 pm, there are, but not many, observations with densities higher than 30 vehicles per km, so we consider most vehicles were travelling in smooth and confident maneuvers. However, traffic at 6 pm at location A was a contrast, with a large proportion of observations distributed with high density and low speed, so this is a rush hour situation.

Patterns for location A and location B are not exactly the same, and this might because a camera is only for surveillance of one side of highway, plus the fact that camera 1106 is at the side of location A which is more congested during afternoon rush hour, and camera 1134 occupies the side of location B that accommodates morning crowds.

Also from above figure 4.5 we see importance of applying weights to aggregated observation points. Take noon sample at location B as an example, the red point with density at 39 vehicles per km is aggregated from only 1 raw observation, while another red point at 16 vehicles per km is aggregated from 33 raw observations, so intuitively these two points should have different affects on shape of a flow model. As we are using number of raw observations an aggregated point calculated from as corresponding weight, different situations, especially those like 3 pm sample here, have reasonable input to a calibration algorithm.

4.3.2 Convergence Speed for Bisection Method

Though bisections is not the most advanced numerical analytical method, consider its time complexity as $O(log_2 n)$, it meets our requirement of performing in real-time

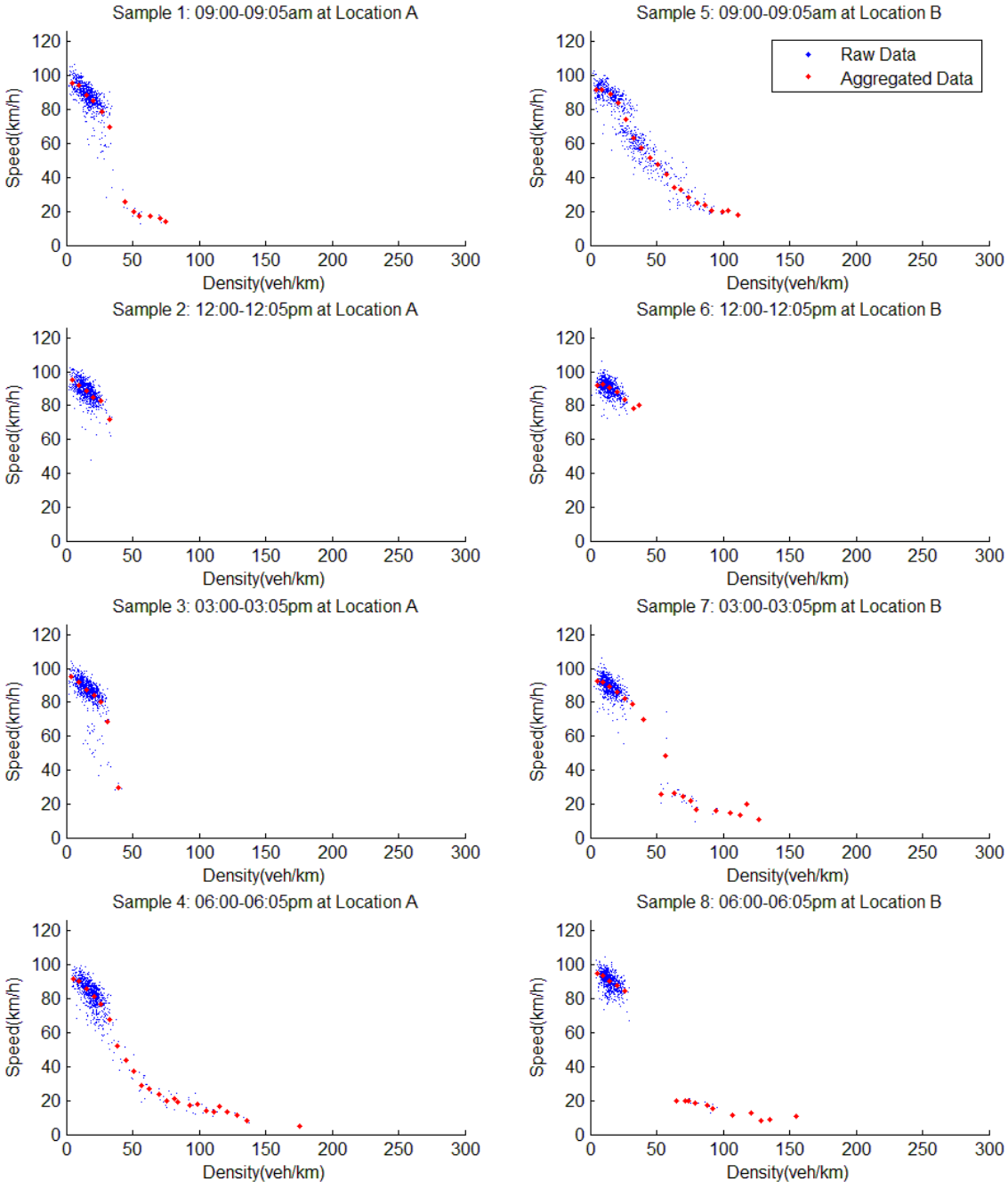

Figure 4.5 Raw and aggregated observation points

for transportation engineering and administration purpose. As shown in figure 4.6, to calibrate against the location B 9 am sample data, every parameter of LCM model converges in at most 12 iterations, so it's guaranteed running time is less than a second. Compared to other non-numerical methods, it's a very fast algorithm for calibrating traffic flow models, and practically this calculating system reacts in real-time.

4.3.3 Calibration Result

In the following table 4.3, we get quantified patterns for sample data sets by calibrating LCM model. As we assumed, parameters of LCM model appear to be consistent for a specific location, and for these two cases, as there are both near-straight sections without any obvious curve, there is no significant difference between values of their parameters. Driving patterns at location A is especially more consistent compared to that of location B, considering location B is near to conjunction of route 285 and route 400, so there are more interference come from the complicated structure of this conjunction.

Table 4.3 Calibration results for sample data sets by bisection based algorithm

Samples		**Parameters**			
		Free Flow Speed (km/h)	Vehicle Length (m)	P-R Time (sec)	Aggression (s^2/m)
Location A	**9:00-9:05 am**	96.1628	4.5088	1.2438	-0.0305
	12:00-12:05 pm	95.6600	4.5088	1.3331	-0.0311
	3:00-3:05 pm	96.4143	4.5029	1.2892	-0.0301
	6:00-6:05 pm	96.6655	4.5029	1.1903	-0.0300
Location B	**9:00-9:05 am**	95.4087	4.4971	1.1544	-0.0310
	12:00-12:05 pm	98.1741	4.4912	1.2240	-0.0286
	3:00-3:05 pm	95.9115	4.4971	1.2592	-0.0305
	6:00-6:05 pm	97.6712	4.5029	1.1720	-0.0290

Thus calibration result of our algorithm meets common sense, and the following figure 4.7 demonstrates how speed-density curve of LCM model fits field data after

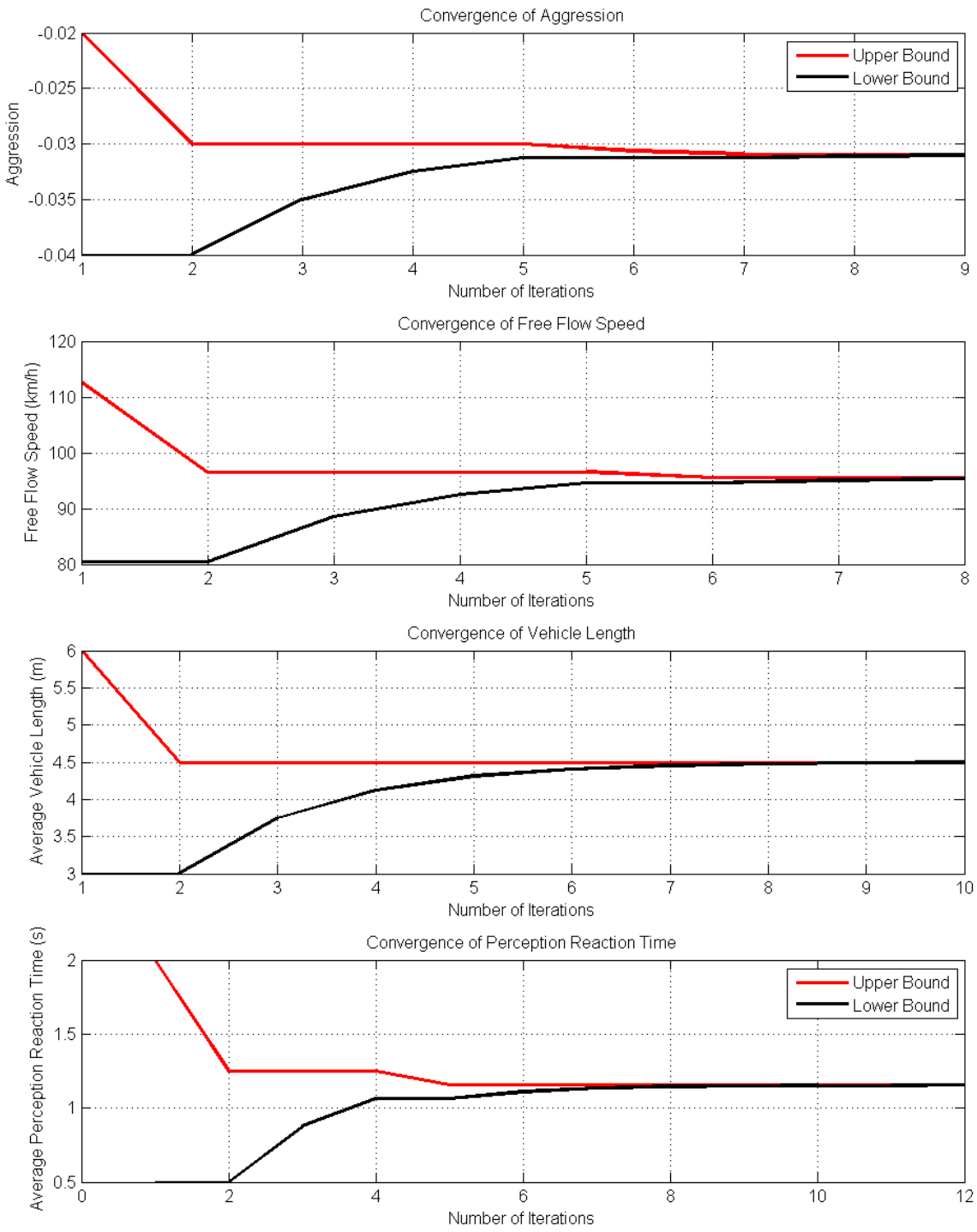

Figure 4.6 Steps for parameters to converge in bisection calibrating method

calibration. This figure further proves role of weighting aggregated points as discussed in section 4.3.1, especially in sample 1 for location A at 9 am, six red points between density 40 and 75 vehicles per km are considered less important so curve of final result doesn't go through these points perfectly, however this makes overall precision of the model optimized.

A more comprehensive visualized result for this bisection based algorithm is shown in a following pate in figure 4.8. Sample 2 for location B at 9 am is opted for this demonstration because its data points are better spread, thus it's easier to read how calibration results fit field and aggregated data. Also Newell's model is calibrated to prove versatility of our algorithm.

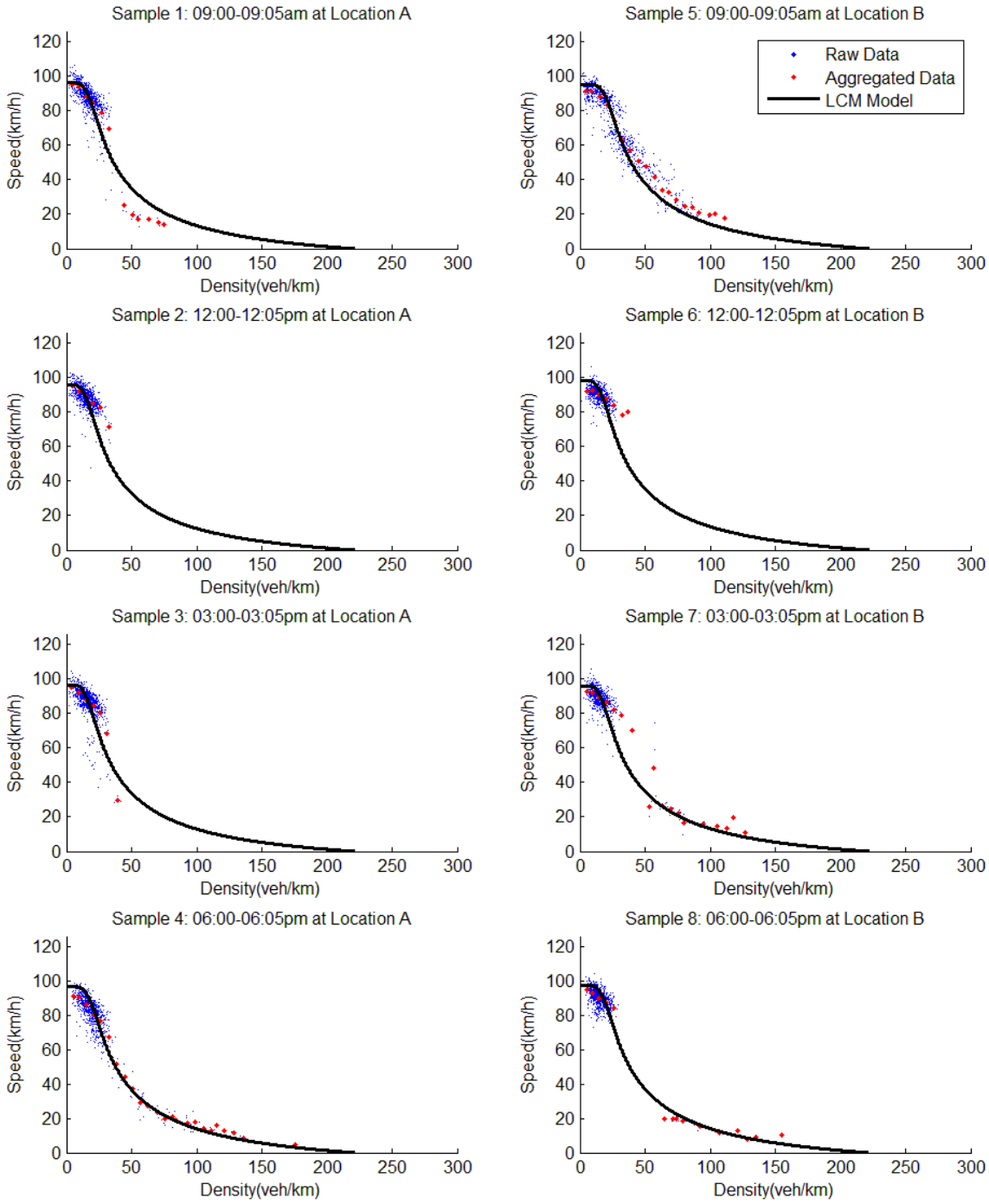

Figure 4.7 Speed-Density curve of LCM model calibrated by bisection based algorithm

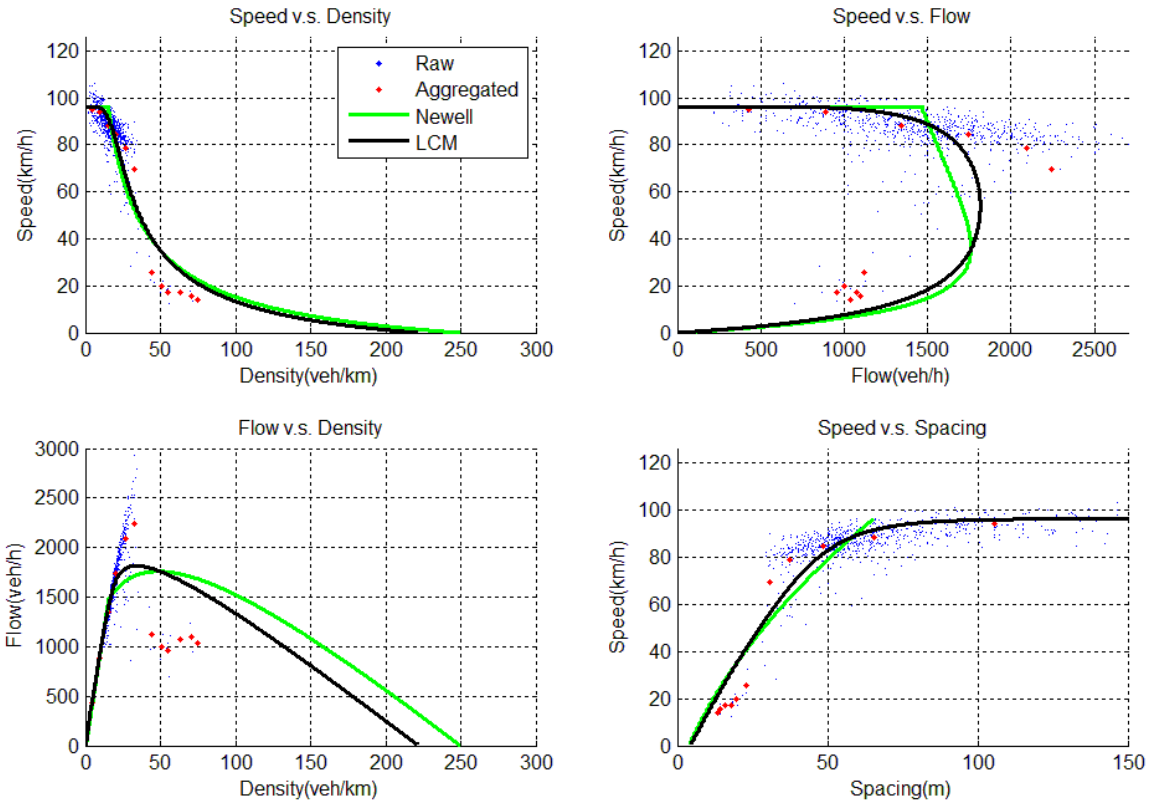

Figure 4.8 LCM and Newell's model calibrated by bisection algorithm

CHAPTER 5

CONCLUSIONS

This thesis demonstrates our research work focusing on quantifying the interaction between human factor parameters and traffic flow characteristics. Three parts of work constitute this thesis: a traffic data extraction algorithm, an efficient calibration algorithm for calculating human factor parameters from empirical traffic data, and a distribution transformation model for determining impact of human factor parameters on traffic flow.

In order to utilize NGSIM trajectory data sets, the data extraction algorithm is proven to produce reliable lane changing information lists extracted from the input NGSIM trajectory data set. By visualizing the lane changing maneuver lists, speed patterns of lane-changing vehicles can be qualitatively found. Further quantitative examination proves the descending and then ascending pattern on speed is solid. Proportions of naneuvers with different descending rates and ascending rates in the full left shifting list are investigated. As part of this investigation, more than half of all lane changing maneuvers toward left meet this criterion, when parameters are set at a reasonable level, that descending rate $a \geq 0.9$ and ascending rate $b \leq 1.2$.

Consider its time complexity as $O(log_2 n)$, the bisection based algorithm demonstrated in section 3.3 has a theoretical high performance. In practise, we run this algorithm on a personal laptop with a T7300 CPU and 2 GB ram, calibration for LCM model against every sample completes in 0.5 second, and calibration for Newell's model runs for less than 1 second. Also because of aggregation procedure, this algorithm is not sensitive to size of sample, as it calibrates both models against a 24

hour data set with 56,000 observations in less than 2 seconds. Also by verifying and analysing the algorithm's procedures and results in section 4.3, we see it has good accuracy in both calculating parameters of a model and drawing statistical relationships between traffic flow, density and speed. Thus it's reasonable to use this calibration algorithm on real-time surveillance of drivers' behaviours.

Using connected vehicle technology as an example, the potential impact of enhanced P-R time on traffic flow was explored from a modeling and statistical perspective. It is anticipated that connected vehicle technology will enhance driver performance in two ways. One is reduced P-R time due to early warning offered by the technology. The other is less variation in response among drivers since the impaired drivers tend to benefit more from the technology than skilled ones. The enhanced P-R time allows drivers to follow closer at the same speed without compromising safety, and hence results in increased flow and capacity.

The role and effect of P-R time on traffic flow was analyzed through a set of car-following models which are progressively more complicated and realistic. To examine the impact of P-R time on flow, these microscopic models were translated to their corresponding macroscopic forms. As a result, functional relationships between flow and P-R time are established. These relationships were then compared with empirical data under varying P-R time values, and the results provide qualitative and quantitative support to the effect of P-R time on flow and capacity.

To evaluate the impact of enhanced P-R time on flow, the ideal approach would be to analyze empirical data collected from real systems of connected vehicles. Given that such an approach is not practical at this time, we pursued a statistical approach where a methodology was developed so that analysts may customize it according to their specific nature and use it to quantify flow benefits before large-scale investment on connected vehicle technology is made.

The proposed methodology makes use of distribution transformation, based on which properties of traffic flow with enhanced P-R time can be directly calculated by inserting new P-R time into a flow distribution. Numerical application is devised to demonstrate the proposed methodology and estimation results are provided in terms of increased flow.

Monte Carlo simulation results reveal that the flow with enhanced P-R time has increased compared to that without enhancement. The enhanced flow has a larger mean and a smaller variance, which suggests that P-R time enhancement by connected vehicle technology can potentially improve traffic flow to a higher and more consistent level without modifying existing facilities.

BIBLIOGRAPHY

2009a, Autoscope Solo Terra Vehicle Detection System, Image Sensing Systems, Inc.

2009b, Autoscope Terra Software User's Guide, Image Sensing Systems, Inc.

2010, Autoscope Solo Terra Video Detection System

Abdel-Aty, M. A., Kitamura, R., & Jovanis, P. P. 1997, Transportation Research Part C: Emerging Technologies, 5, 39

Agarwal, V., Murali, N. V., & Chandramouli, C. 2009, IEEE transactions on intelligent transportation systems, 10, 486

Agency, U. E. P. 2014

Antonisse, R. W., Daly, A. J., & Ben-Akiva, M. 1989, Transportation Research Record

Biswas, S., Tatchikou, R., & Dion, F. 2006, Communications Magazine, IEEE, 44, 74

Brackstone, M. & McDonald, M. 1999, Transportation Research Part F: Traffic Psychology and Behaviour, 2, 181

Casella, G. & Berger, R. L. 2001 (Duxbery)

Chandler, R. E., Herman, R., & Montroll, E. W. 1958a, Operations Research, 165

—. 1958b, Operations Research, 165

Chen, H.-K. & Hsueh, C.-F. 1998, Transportation Research Part B: Methodological, 32, 219

Coifman, B., Beymer, D., McLaunchlan, P., & Malik, J. 1998, Transportation Research Part C: Emerging Technologies, 4, 271

Cunto, F. & Saccomanno, F. F. 2008, Accident Analysis and Prevention, 1171

Daganzo, C. F. 1994, Transportation Research Part B: Methodological, 28, 269

Dalal, N. & Triggs, B. 2005, IEEE Conference on Computer Vision and Pattern Recognition (CVPR)

Darbha, S. & Rajagopal, K. R. 1999, Transportation Research Part C:Emerging Technologies, 7, 329

Donmez, B., Boyle, L. N., & Lee, J. D. 2007, Accident Analysis & Prevension, 39, 581

D.Prabhu, G. & Tessier, R. G. 2011, Master's thesis, University of Massachusetts, Amherst

Duret, A., Buisson, C., & Chiabaut, N. 2008, Transportation Research Record: Journal of the Transportation Research Board, 188

Faghri, A. & Hamad, K. 2002, Canadian Journal of Civil Engineering, 29, 325

FHWA. 2006a, Next Generation SIMulation fact sheet: NGSIM Overview, http://www.fhwa.dot.gov/publications/research/operations/its/06135/index.cfm

—. 2006b, Next Generation Simulation (NGSIM), http://ops.fhwa.dot.gov/trafficanalysistools/ngsim.htm

—. 2011, How Do Weather Events Impact Roads?

for Statistics, N. N. C. & Analysis. 2010, Traffic Safety Facts 2009 Data, Pedestrians Part, Tech. rep., National Highway Traffic Safety Administration, U.S. Department of Transportation

Forbes, T. W. & Simpson, M. E. 1968, Transportation science, 2, 77

Gazis, D. C., Herman, R., & Potts, R. B. 1959, Operations Research, 499

Gipps, P. 1981, Transportation Research Part B: Methodological, 15, 105111

Greenshields, B. D., Bibbins, J. R., Channing, W. S., & Miller, H. H. 1935, Highway Research Board Proceedings, 14, 448

Gurusinghe, G. S., Nakatsuji, T., Azuta, Y., Ranjitka, P., & Tanaboriboon, Y. 2002, Transportation Research Record: Journal of the Transportation Research Board, 166

H.-S. Tan, R. Rajamani, a.-B. Z. 1998, Proceedings of the American Control Conference

Herman, R. & Potts, R. B. 1959, In: Proceedings of the Symposium on Theory of Traffic Flow, 147

Hoogendoorn, S. P., Zuylen, H. J. V., Schreuder, M., Gorte, B., & Vosselman, G. 2004, Transportation Research Record: Journal of the Transportation Research Board, 121

Kanhere, N. K., Birchfield, S. T., & Sarasua, W. A. 2006, Transportation Research Record, 1944, 89

Kesting, A. & Treiber, M. 2008, Transportation Research Record: Journal of the Transportation Research Board, 2088, 148

Kikuchi, S. & Chakroborty, P. 1992, Transportation Research Record, 82

Kobayashi, T., Hidaka, A., & Kurita, T. 2008, ICONIP 2007, Part II, 598

Kometani, E. & Sasaki, T. 1959, In: Proceedings of the Symposium on Theory of Traffic Flow, 105

Kosonen, I. 1999, Master's thesis, HELSINKI UNIVERSITY OF TECHNOLOGY

Koutsopoulos, H. N., Lotan, T., & Yang, Q. 1994, Transportation Research Part C: Emerging Technologies, 2, 91

L.Alonso, C, T.-F., & J.P., O. 2011, Sensors, 11

Laval, J. A. & Leclercq, L. 2010, Philosophical Transactions of The Royal Society, 4519

Lenart, L., Tomsic, M., Kusar, J., & StarbekArdeshir, M. 2002, Canadian Journal of Civil Engineering, 29, 325

Liu, H. X., He, X., & Recker, W. 2007, Transportation Research, Part B vol:41, 448

Lyman, S., Ferguson, S. A., Braver, E. R., & Williams, A. F. 2002, Injury Prevension, 8, 116

Maycock, G., Brocklebank, P. J., & Hall, R. D. 1998, Transport Research Laboratary Report

Michalopoulos, P. G. 1991, IEEE transactions on vehicular technology, 40, 21

Michaud, F., Lepage, P., Frenette, P., Letourneau, D., & Gaubert, N. 2006, IEEE Transactions on Intelligent Transportation Systems, 7, 437

Nasar, J., Hecht, P., & Wener, R. 2008, Accident Analysis & Prevension, 40, 69

Nekoui, M., Pishro-Nik, H., & Ni, D. 2011, International Journal of Vehicular Technology

Newell, G. 1961, Operations Research, 2, 209

—. 1993, Transportation Research Part B: Methodological, 4, 289303

Ni, D. 2006, Proceedings of the 2006 Winter Simulation Conference

—. 2011a, ASCE-ICCTP 2011

—. 2011b, ASCE-ICCTP 2011

Ni, D., Li, J., Andrews, S., & Wang, H. 2012, International Journal of Vehicular Technolgoy

Nilsson, G. 2004, Lund Institute of Technology and Society, Traffic Engineering

Peden, M., Scurfield, R., Sleet, D., Mohan, D., Hyder, A. A., Jarawan, E., & Mathers, C. 2004, World Report on Road Traffic Injury Prevention, Tech. rep., World Health Organization

Perrine, M. N., Waller, J. A., & Harris, L. S. 1971, DOT HS-800 599 Final Report

Pigman, J. G. & Agent, K. R. 1990, Transportation Research Record, 12

Polydoropoulou, A., Ben-Akiva, M., & Kaysi, I. 1994, Transportation Research Record

Punzo, V. & Simonelli, F. 2005, Transportation Research Record: Journal of the Transportation Research Board, 53

Quimby, A., Maycock, G., Palmer, C., & Buttress, S. 1999, Transport Research Laboratary Report

Rakha, H. & Arafeh, M. 2010, Transportation Science, 44, 151

Ran, B., Hall, R. W., & Boyce, D. E. 1996, Transportation Research Part B: Methodological, 30, 31

Royal, D. 2003, DOT HS 809 566 Report

Schultz, G. G. & Rilett, L. 2004, Transportation Research Record: Journal of the Transportation Research Board, 1876, 41

Shinar, D., Schechtman, E., & Compton, R. 2001, Accident Analysis & Prevension, 33, 111

Stamatiadis, N. & Deacon, J. A. 1995, Accident Analysis & Prevension, 27, 443

Taylor, M. A. P., D'Este, G. M., & Zito, R. 1999, Computer-Aided Civil and Infrastructure Engineering, 255

Thiemann, C., Treiber, M., & Kesting, A. 2008, Transportation Research Record, 90

Treiterer, J. & Mayers, J. A. 1974, In: Proceedings of the Sixth International Symposium on Transportation and Traffic Theory, 13

Vahidi, A. & Eskandarian, A. 2003, IEEE Transactions on Intelligent Transportation Systems, 4, 132

van Arem, B., van Driel, C., & Visser, R. 2006, IEEE Transactions on Intelligent Transportation Systems, 7, 429

VanderWerf, J., Shladover, S., Miller, M., & Kourjanskaia, N. 2001, Pre-Print CD-ROM of 81st TRB Annual Meeting

Viola, P. & Jones, M. 2008, Proc. of IEEE Computer Vision and Pattern Recognition, Kauai, 511

Wagenaar, A. C. 1986, Journal of Safety Research, 17, 101

Wasson, J. S., Sturdevant, J. R., & Bullock, D. M. 2008, ITE Journal, 20

Weinfeld, A. 2010, 17th ITS World Congress, Busan, 2010: Proceedings

Williams, A. F. & Carsten, O. 1989, American Journal of Public Health, 79, 326

Xing, J. 1995, In: Proceedings of the Second World Congress on ATT, 1739

Xu, Q., Sengupta, R., & Jiang, D. 2003, Vehicular Technology Conference

Yang, J.-S. 2005, American Control Conference, 2128

Yeo, H., Skabardonis, A., Halkias, J., Colyar, J., & Alexiadis, V. 2008, Transportation Research Part C: Emerging Technologies, 68